*REVISED Manuscript (text UNmarked)
Click here to view linked References

Solution equilibria of cytosine- and guanine-rich sequences near the promoter region of the *n-myc* gene that contain stable hairpins within lateral loops

Sanae Benabou[1], Rubén Ferreira[2], Anna Aviñó[2], Carlos González[3], Sébastien Lyonnais[4], Maria Solà[4], Ramon Eritja[2], Joaquim Jaumot[1], Raimundo Gargallo[1*]

1. Solution Equilibria and Chemometrics Group, Department of Analytical Chemistry, University of Barcelona, Diagonal 645, E-08028 Barcelona, Spain

2. Institute for Advanced Chemistry of Catalonia (IQAC-CSIC), CIBER-BBN Networking Centre on Bioengineering, Biomaterials and Nanomedicine, Jordi Girona 18-26, E-08034 Barcelona, Spain

3. Institute of Physical Chemistry "Rocasolano", CSIC, Serrano 119, E-28006 Madrid, Spain

4. Department of Structural Biology, Molecular Biology Institute of Barcelona (IBMB-CSIC), Baldiri Reixac 4-8, 08028 Barcelona, Spain

* Corresponding author

Tel: (34)-934039274

Fax: (34)-934021233

e-mail address: raimon_gargallo@ub.edu

Abstract

BACKGROUND

Cytosine- and guanine-rich regions of DNA are capable of forming complex structures named *i*-motifs and G-quadruplexes, respectively. In the present study the solution equilibria at nearly physiological conditions of a 34-bases long cytosine-rich sequence and its complementary guanine-rich strand corresponding to the first intron of the *n-myc* gene were studied. Both sequences, not yet studied, contain a 12-base tract capable of forming stable hairpins inside the *i*-motif and G-quadruplex structures, respectively.

METHODS

Spectroscopic, mass spectrometry and separation techniques, as well as multivariate data analysis methods, were used to unravel the species and conformations present.

RESULTS

The cytosine-rich sequence forms two *i*-motifs that differ in the protonation of bases located in the loops. A stable Watson-Crick hairpin is formed by the bases in the first loop, stabilizing the *i*-motif structure. The guanine-rich sequence adopts a parallel G-quadruplex structure that is stable throughout the pH range 3 - 7, despite the protonation of cytosine and adenine bases at lower pH values. The presence of G-quadruplex aggregates was confirmed using separation techniques. When mixed, G-quadruplex and *i*-motif coexist with the Watson-Crick duplex across a pH range from approximately 3.0 to 6.5.

CONCLUSIONS

Two cytosine- and guanine-rich sequences in *n-myc* gene may form stable *i*-motif and G-quadruplex structures even in the presence of long loops. pH modulates the equilibria involving the intramolecular structures and the intermolecular Watson-Crick duplex.

GENERAL SIGNIFICANCE

Watson-Crick hairpins located in intramolecular G-quadruplexes and *i*-motifs in the promoter regions of oncogenes could play a role in stabilizing these structures.

Keywords: G-quadruplex, *i*-motif, quadruplex / duplex competition, *n-myc*, chromatography, multivariate analysis

Introduction

Cytosine-rich regions of DNA are capable of forming a characteristic structure known as an *i*-motif. The core of this structure is formed by the binding of two cytosine bases via three hydrogen bonds. The key characteristic is that one of the cytosines involved in the base pair must be protonated at N3. Given this requirement, *i*-motif structures can only be formed at a pH lower than 7, their maximal stability being found at pH values around 4.5, i.e., near the pK_a of free cytosine. The formation of *i*-motif structures *in vitro* has been proposed in sequences corresponding to the cytosine-rich strand of telomeric DNA [1, 2], the human centromeric satellite III [3], and genes such as *VEGF* [4], *bcl-2* [5], *k-ras* [6], *RET* [7], *c-myc* [8], *c-jun* [9], and *Rb* [10]. Despite the requirement of an acidic medium for high stability, the potential role of *i*-motif structures in the control of gene expression is being investigated [8]. Furthermore, the structural properties of the *i*-motif have attracted interest due to their potential applications in nanotechnology [11, 12].

Cytosine-rich regions are accompanied by the corresponding complementary guanine-rich regions, which may form a special structure known as the G-quadruplex. The core of this structure is formed by two or more tetrads, an ensemble of four guanine bases linked by hydrogen bonds in almost the same spatial plane. The *in vitro* formation of such structures in DNA sequences corresponding to the end of telomeres [13] and to the promoter regions of several oncogenes [14, 15] has previously been reported, and recently, the existence of G-quadruplexes *in vivo* has also been shown [16]. Efforts are being made to develop drugs that could selectively bind to G-quadruplex structures, in turn modulating the expression of certain genes [17].

In vivo, the coexistence of both guanine-rich and cytosine-rich strands suggests the formation of the Watson-Crick duplex as the major species, the proportion of the intramolecular structures (*i*-motif and G-quadruplex) being residual, if any. Nevertheless, efforts are being made to quantify the formation of the duplex structure in mixtures of guanine- and cytosine-rich regions in order to determine the potential role of these minority structures in gene expression [18, 19].

In this context, we focused our attention on two cytosine- and guanine-rich sequences located near the promoter region of the *n-myc* gene which have not been studied to date. This gene is a member of the *myc* family of transcription factors and encodes a protein with a basic helix-loop-helix domain. Amplification of this gene is associated with a variety of tumors, most notably neuroblastoma [20]. The cytosine-rich sequence studied (nmyc01,

Table 1) herein is located at -349 to -315 bases upstream of the first position of the coding region (CDS), being the guanine-rich sequence complementary to nmyc01 (nmyc02, Table 1). These sequences are unique because they show an unusual 12-bases long loop containing two complementary TGAC sequences which, in principle, could hinder the formation of stable intramolecular structures [21]. To our knowledge, no previous work has been done on these sequences. Recently, it was proposed that another guanine-rich sequence, located in the first intron of the *n-myc* sequence, forms both monomeric and dimeric G-quadruplex structures [22]. A G-quadruplex-duplex structure has also been hypothesized in a thrombin-binding aptamer, although in this case the sequence is an artificial sequence obtained from SELEX [23].

Circular Dichroism (CD), molecular fluorescence based on molecular beacons, Nuclear Magnetic Resonance (NMR), polyacrylamide gel electrophoresis (PAGE) and molecular absorption spectroscopy were used to monitor the experiments carried out. Multivariate data analysis methods were used to recover qualitative and quantitative information about the species and conformations present in all experiments. Finally, Electrospray Ionization-Mass Spectrometry (ESI-MS) and Size-Exclusion Chromatography (SEC) were used to complement the results obtained from spectroscopy and PAGE [24].

Materials and methods

Reagents

The DNA sequences (Table 1) were synthesized on an Applied Biosystems 3400 DNA synthesizer using the 200 nmols scale synthesis cycle. Standard phosphoramidites were used. Ammonia deprotection was performed overnight at 55^{o}C. The resulting products were purified using Glen-Pak Purification Cartridge (Glen Research). The length and homogeneity of the oligonucleotides was checked by denaturing polyacrylamide gel electrophoresis (PAGE) and reversed-phase HPLC using X-Terra® columns. The quencher Q was introduced at the 3'-end of the sequence Fnmyc02Q using a dabsyl-CPG solid support (Glen Research) and the fluorophore F at the 5'-end using the fluorescein phosphoramidite Fluoroprime (Amersham Biosciences). DNA strand concentration was determined by absorbance measurements (260 nm) at 90^{o}C using the extinction coefficients calculated using the nearest-neighbor method as implemented on the OligoCalc webpage [25]. Before any experiment, DNA solutions were first heated to

90°C for 10 minutes and then allowed to reach room temperature. KCl, KH_2PO_4, K_2HPO_4, $NaCH_3COO$, HCl and NaOH (a.r.) were purchased from Panreac (Spain). MilliQ ® water was used in all experiments.

Procedures

Absorbance spectra were recorded on an Agilent 8453 diode array spectrophotometer. The temperature was controlled by means of an 89090A Agilent Peltier device. Hellma quartz cells (1 or 10 mm path length, and 350, 1500 or 3000 μl volume) were used. CD spectra were recorded on a Jasco J-810 spectropolarimeter equipped with a Julabo F-25/HD temperature control unit. Hellma quartz cells (10 mm path length, 3000 μl volume) were used. pH was measured using an Orion SA 720 pH/ISE meter and a micro-combination pH electrode (Thermo). Fluorescence emission spectra were recorded on an Aminco Bowman AB-2 fluorimeter, equipped with a cell holder, the temperature of which was controlled using a JP Selecta Frigiterm bath. Emission spectra were recorded between 500 and 620 nm and fluorescence intensities were recorded every 1 nm. The excitation wavelength was set to 492 nm, the photomultiplier voltage to 600 V and the excitation and emission band pass to 4 nm. A 10 mm pathlength and 400 μL volume quartz cell was used.

Acid-base titrations were monitored either in-line (taking advantage of the stirrer incorporated in the Agilent cell holder) or at-line (in the case of the CD instrument). Experimental conditions were as follows: 25°C and 150 mM KCl. Titrations were carried out by adjusting the pH of solutions containing the oligonucleotides. CD and/or absorbance spectra were recorded in a pH stepwise fashion.

Melting experiments were monitored using the Agilent-8453 spectrophotometer equipped with a Peltier unit. The DNA solution was transferred to a covered 10-mm-path-length cell and absorption spectra were recorded at 1°C intervals with a hold time of 3 min at each temperature, which yielded an average heating rate of approximately 0.3°C min^{-1}. Buffer solutions were 20 mM phosphate or acetate, and 150 mM KCl. Each sample was allowed to equilibrate at the initial temperature for 30 minutes before the melting experiment began.

NMR spectra were acquired in a Bruker Advance spectrometer operating at 600 MHz and equipped with a cryoprobe. Water suppression was achieved by the inclusion of a WATERGATE [26] module in the pulse sequence prior to acquisition.

ESI-MS spectra were acquired in a Synapt HDMS (Waters, Manchester, UK) under the following instrumental conditions: flow (15 μL·min^{-1}), capillary potential (2.4 kV), temperature source (100^{o}C), desolvation temperature (100^{o}C), cone voltage (45 V) and extraction cone (5 V).

The chromatographic system consisted of an Agilent 1100 Series HPLC instrument equipped with a G1311A quaternary pump, a G1379A degasser, a G1392A autosampler, a G1315B photodiode-array detector furnished with a 13-μL flow cell, and an Agilent Chemstation for data acquisition and analysis (Rev. A 10.02), all from Agilent Technologies (Waldbronn, Germany). A BioSep-SEC-S 2000 column (300x7.8 mm, particle size 5 μm and pore size 145 Å) from Phenomenex (Torrance, CA, USA) was used for the chromatographic separation. The mobile phase was 75mM potassium phosphate adjusted to pH 7.1. The flow rate was set to 1.0 mL/min. A volume of 15 μL of the sample was injected and the temperature was set to 25^{o}C [27]. Absorbance spectra were recorded between 200 and 500 nm.

Polyacrylamide gel electrophoresis was performed at room temperature on 12% non-denaturing gels (19:1 acrylamide:bisacrylamide, Sigma) of 10x10.5cm with a miniVE apparatus (Hoeffer) at 10V/cm for 2 hours. Gels and buffers contained 40mM Tris Acetate pH 5.2 or 40mM Tris Acetate pH 8.0. 100 pg of each oligonucleotide were loaded per lane after addition of 10% (w/v) of a loading dye containing 30% Glycerol and 0.1% Bromophenol Blue. After migration, the gels were stained with SYBr Gold (Molecular Probes) according to manufacturer's instructions and digitalized with a Typhoon 8600 system (Molecular Dynamics).

Data analysis

Spectra recorded during acid-base or melting experiments were arranged in a table or data matrix **D**, with *m* rows (spectra recorded) and *n* columns (wavelengths measured). The goal of data analysis was the calculation of distribution diagrams and pure (individual) spectra for all *nc* spectroscopically-active species considered throughout an experiment. The distribution diagram provides information about the stoichiometry and stability of the species considered (in the case of acid-base and mole-ratio experiments), as well as the thermodynamics of the melting processes. In addition, the shape and intensity of the pure spectra may provide qualitative information about the structure of the species. With this goal in mind, data matrix **D** was decomposed according to Beer-Lambert-Bouer's law in matrix form:

$$\mathbf{D} = \mathbf{C}\,\mathbf{S}^{T} + \mathbf{E} \qquad (1)$$

where **C** is the matrix (*m* x *nc*) containing the distribution diagram, $\mathbf{S}^T$ is the matrix (*nc* x *n*) containing the pure spectra, and **E** is the matrix of data (*m* x *n*) not explained by the proposed decomposition.

The mathematical decomposition of **D** into matrices **C**, $\mathbf{S}^T$, and **E** may be conducted in two different ways, depending on whether a physico-chemical model is initially proposed (hard-modeling approach) or not (soft-modeling approach) [28]. For hard-modeling approaches, the proposed model depends on the nature of the process under study. Hence, for acid-base experiments the model will include a set of chemical equations describing the formation of the different acid-base species from the neutral species, together with approximate values for the stability constants, such as the following:

$$DNA + pH^+ \leftrightarrow DNA{\cdot}H_p \qquad Beta_{1p} = [DNA{\cdot}H_p] / [DNA]\,[H^+]^p \qquad (2)$$

In this equation, the parameter *p* is related to the Hill coefficient and describes qualitatively the cooperativity of the equilibrium. Values of *p* greater than 1 indicate the existence of a cooperative process.

For melting experiments, the physico-chemical model is related to the thermodynamics of DNA unfolding. Hence, for the unfolding of intramolecular structures such as those studied here, the chemical equation and the corresponding equilibrium constant may be written as:

$$DNA_{\ folded} + heat \leftrightarrow DNA_{\ unfolded} \qquad K_{unfolding} = [DNA_{\ unfolded}] / [DNA_{\ folded}] \qquad (3)$$

For melting experiments, the concentration of the folded and unfolded forms is temperature-dependent. Accordingly, the equilibrium constant depends on temperature according to the van't Hoff equation:

$$\ln K_{\ unfolding} = - \Delta H_{vH} / RT + \Delta S_{vH} / R \qquad (4)$$

In this case it is assumed that ΔH_{vH} and ΔS_{vH} will not change throughout the range of temperatures studied here.

Whenever a physico-chemical model is applied, the distribution diagram in **C** complies with the proposed model. Accordingly, the proposed values for the equilibrium constants and the shape of the pure spectra in $\mathbf{S}^T$ are refined to explain satisfactorily data in **D**, whereas residuals in **E** are minimized.

In this study, hard-modeling analysis of acid-base and mole-ratio experiments used the EQUISPEC program [29]. Hard-modeling of melting experiments was conducted using a modified version of the Multivariate Curve Resolution-Alternating Least Squares (MCR-ALS) procedure, which includes the model proposed in equation (4) for the unfolding of intramolecular structures [30].

Results

The solution equilibria of the cytosine-rich region were studied first. Those of the guanine-rich region were then considered. Finally, the potential formation of the Watson-Crick duplex structure from the isolated structures was examined.

Solution equilibria of the cytosine-rich region

To study the influence of pH on the conformational equilibria of nmyc01, acid-base titrations and melting experiments were carried out. An acid-base titration of an nmyc01 sample in the pH range 2.0–7.3 was simultaneously monitored using CD and molecular absorption spectroscopy. A selected set of the measured CD and absorption spectra is shown in Figure 1a-b and the whole set of experimental spectra is presented in Figure S1 (Supplementary Material). At pH values around 6, the strongly positive band around 286 nm is indicative of the formation of an *i*-motif structure [31]. To obtain quantitative information the whole set of experimental CD and molecular absorption spectra were analyzed using a multivariate data analysis method, which enabled calculation of the distribution diagram and pure spectra for each of the acid-base species considered. The results obtained depend strongly on the number of acid-base species considered to be present during the titration. In this case, the analysis was performed on the assumption of the presence of three or four acid-base species. After a careful study of fitted curves and of the resulting residuals, the presence of four acid-base species was proposed, i.e., three transitions throughout the pH range considered. The obtained fits for the acid-base models considering three or four species are shown in the Supplementary Material (Figure S1).

The calculated distribution diagram and pure spectra are shown in Figure 1c-e. The information contained in both plots helps us to explain each of the four proposed acid-base species. The first species, present at a pH higher than 6, would correspond to the neutral form where all bases are deprotonated (i.e., in their neutral form). Its spatial structure is probably a partially stacked single strand. The two major species at pH 5.8 and 3.0 would correspond to two *i*-motif structures (named *i*-motif 1 and *i*-motif 2, respectively) stabilized by cytosine^{+}·cytosine base pairs. The calculated pure CD spectra for these two species are characteristic of this structure, showing a strong positive band around 285 nm and a weaker negative band around 264 nm. Finally, the major species at pH values lower than 2.0 would correspond to species in which all (or almost all) cytosines and adenine bases are protonated.

As expected, the formation of the *i*-motif 1 structure from the neutral form takes place within a narrow pH range (Figure 1c). In this case, the value for parameter *p* (equation 2) is 3, in concordance with the observed cooperativity. Similarly, the disruption of the *i*-motif 2 to yield the fully protonated DNA occurs within a very narrow pH range, with a *p* value equal to 4, and only in a strongly acidic medium. This can be explained by the resistance of the bases involved in the *i*-motif core to their protonation, which destroys their structure. On the contrary, the transition between both *i*-motifs is smooth (*p* value equal to 1) with an apparent pK_a around 4.1. Overall, the existence of two *i*-motifs can be attributed to the protonation of cytosine (pK_a around 4.3) and/or adenine (pK_a around 3.5, [32]) bases present in the loops. The pure absorption spectrum for *i*-motif 2 is slightly shifted to longer wavelengths (Figure 1e), as a result of protonation. Concomitantly, the pure CD spectra of both *i*-motifs are similar because the core structure is well maintained, despite protonation (Figure 1d). As these bases are not involved in the formation of the C^+·C core and probably do not form any base pairs, their protonation does not have any cooperative effect.

The nature of the species proposed from the spectroscopically-monitored acid-base titration was also studied using ^{1}H NMR (Figure 2, left). At pH 7 and 5^{o}C, the presence of signals between 12.5 and 14 ppm indicates the formation of Watson-Crick base pairs in nmyc01 [33]. The number of imino signals observed is consistent with the formation of two A·T and two G·C base pairs, thus association in antiparallel orientation of the TGCA repeats of the long loop. The characteristic signals of protonated cytosines (~15 ppm) are not observed at this pH. These facts suggest that the structure of the previously proposed neutral strand at pH 7 is stabilized by Watson-Crick base pairs. At pH 5 and 5^{o}C, the signals related to the Watson-Crick base pairs are weaker and broader than at pH 7 whereas a clear signal of imino hydrogen at 15.5 ppm denotes the existence of protonated cytosines. This is in accordance with the co-existence of Watson-Crick and C^+·C base pairs. This latter pairing is also present at pH 4. The large line-width of this imino signal (at 15.5 ppm) at pH 4 is most probably due to the presence of several similar conformers in equilibrium. This is not unexpected since one of the cytosine tracts is shorter than the others.

To study the potential presence of this base pairing between the TGCA repeats in the long loop, NMR spectra of a modified sequence (nmyc01m) were recorded (Figure 2, right). In this case, the second TGCA sequence was replaced by four T, which impedes the formation of the suspected stem-loop structure. At pH 7 and pH 5, the presence of such base pairs was seen dramatically reduced in comparison to the wild sequence nmyc01, which confirmed the absence of a stem. Interestingly, at pH 7 and 5^{o}C, the presence of C^+·C base pairs was detected in the spectrum of nmyc01m, suggesting a stabilization of the i-motif in the mutated sequence. From these results, however, it is not

clear whether the Watson-Crick and C^+·C base pairs in nmyc01 are present in a unique structure (an i-motif including a stem-loop stabilized by Watson-Crick base pairing in the long loop) or in a mixture of several species (an i-motif and the neutral strand stabilized by Watson-Crick base pairing). Melting experiments, as well as separation of the DNA species by polyacrilamide gel electrophoresis, have been carried out to determine the most plausible situation.

The *i*-motif structure may be formed by the unfolding of a unique DNA strand or by the association of individual strands. Given the high number of cytosine bases present in the nmyc01 sequence, both intramolecular folding and intermolecular arrangements can be envisaged. Melting experiments were first conducted to assess the existence of an intramolecular transition and to determine the influence of pH on the stability of the *i*-motif structure. A mathematical procedure was used to analyze the whole set of experimental spectra to obtain information about the number of conformations involved, as well as thermodynamic information related to each individual transition. This procedure is based on the proposal of thermodynamic equations to which spectroscopic data are fitted [30]. As example, the analysis of spectra recorded during a melting experiment at pH 6.1 is included as Supplementary Material (Figure S2). At pH 6.1, the melting temperature (T_m) was invariant throughout the concentration range 0.5-92 μM, which suggested intramolecular folding in the experimental conditions used in this study.

These results suggest that the proposed distribution diagram (Figure 1c) may also be valid for the higher DNA concentrations used in NMR measurements (0.17 and 0.58 mM). Therefore, at pH 5, the Watson-Crick and C^+·C base pairs observed are present in a single species (an i-motif including a hairpin stabilized by Watson-Crick base pairing in the long loop), rather than in a mixture of i-motif and the neutral strand stabilized by Watson-Crick base pairing.

Table 2 summarizes the thermodynamic parameters calculated over the pH range 3.7 – 6.4. As expected for a structure in which the core is formed by protonated bases, the melting of the *i*-motif structure formed by the nmyc01 sequence was strongly pH-dependent (Figure S3). In the pH range 6.4 to 4.5, T_m values were almost a linear function of pH. Previous studies also found these relationships and showed that T_m was highest at a pH around the pK_a of free cytosine, depending on experimental conditions such as ionic strength [31]. The values for the change in enthalpy were maximal around the pK_a of free cytosine. Assuming that the disruption of a C^+·C base pair needs around 11 ± 1 kcal·mol^{-1} [31], it can be deduced that the number of C^+·C base pairs disrupted throughout the pH range 5.8–6.4 is around 5. An increment of the ΔH^0 value was observed at lower pH values, with a maximal value around the pKa of cytosine.

In order to quantify the effect of the Watson-Crick stem on the stability of the *i*-motif, the stability of a mutated sequence (nmyc01m) was studied. The T_m values at pH 5.0 and 6.1 were 61 and 33^{o}C, respectively, similar to those obtained for the wild-type sequence (see Table 2). The changes in enthalpy and entropy, however, were clearly lower than in the first case. As a result, the Gibbs free energy was slightly lower than in the case of the wild-type sequence, especially at pH 5.0.

To gain information about the molecularity and structure of nmyc01 and nmyc01m folding, separation of the DNA species incubated at pH 5.2 and at a moderate strand concentration in presence of 150mM KCl, was realized by PAGE in gels buffered at pH 5.2 or pH 8.0 (Figure 3a). nmyc01 migration at pH 5.2 showed the presence of a single band of lower mobility (lane 2) separated from the unstructured monomer by smearing species. In the same conditions, this band was also found in nmyc01m with the concomitant apparition of 3 others retarded bands (lane 4), however with a lower decrease in the fluorescence of the unstructured monomer as compared with the wild-type sequence (compare the band U in lanes 2 and 3). In both cases, all the up-shifted band disappeared upon heat denaturation or PAGE buffered at pH 8.0 (see lanes 5-8 in the right panel). This first demonstrates the presence of ordered monodisperse DNA structures sensitive to pH, thus i-motifs. Interestingly, the potential to form a stem-loop structure in the long loop in myc01 directs a particular, well stabilized and monodisperse (i.e. with lower conformational fluctuation) DNA structure from diverse choices of high-ordered arrangements when this loop is mutated as in nmyc01m. It is tempting to speculate from these results that the stem-loop dictates a preferred configuration into an intramolecular folding whereas its absence unlocks some possibilities to form dimer, trimers and tetramers associated by protonated cytosines.

The influence of salt content on stability was also studied. At pH 6.1, the *i*-motif structure formed even in the absence of added salt (KCl), as denoted by the characteristic CD signals of the *i*-motif structure (Figure S4). No changes were observed upon later addition of salt. On the contrary, the melting temperature at pH 6.1 decreased from 52^{o}C (without added salt) to 33^{o}C (at 150 mM KCl). This behavior can be attributed to the shift in the pK_a of cytosine to higher values in a low-salt buffer [31].

Solution equilibria of the guanine-rich region

Separation by PAGE of nmyc02 was realized in the same conditions than for nmyc01 (Figure 3B) and revealed a complex migration pattern characteristic of G-rich oligonucleotides, with a mixture of unstructured monomer and

smearing DNA species of high molecular mass, with some diffuse bands and including material blocked in the gel well. Both patterns were identical at pH 5.2 and pH 8. A small up-shift slightly migrating upon the unstructured monomer was however observed (lane 2 and 6) indicating a preferential folded, compact structure, probably intramolecular. The high molecular species were seen resistant to harsh denaturation conditions, such as 15 minutes at 99°C in their incubation buffer containing KCl. The monodisperse band appeared also relatively resistant to these conditions, a signature of G-quadruplex species involving repetitions of 4-5 consecutive guanines. As with nmyc01, nmyc02 presents two TGCA repeats in the long loop, thus suggesting the possible formation of a stem-loop. We thus synthesized an nmyc02m modified in the second TGCA repeat, as in nmyc01m. PAGE separation of this oligonucleotide incubated in the same conditions than nmyc02 indicated the absence of the up-shifted species observed in nmyc02 in the benefit of very diffuse band around and upon the position of the unstructured monomer, associated with high molecular weight smearing species and 3 very diffuse bands, also present with nmyc02, probably indicative of DNA multimers (Figure 3B, lanes 4 and 8). As with nmyc02, these structures were resistant to severe heat denaturation conditions (lanes 4, 8). Such a result strongly supports the idea that the retarded band for nmyc02 could be in this case a stabilized and compact structure folded into an intra-molecular G-quadruplex associated with a stem-loop involving Watson-Crick base-pairs. As with the i-motif, formation of this stem-loop may direct the formation pathway towards the intramolecular species rather than multimers.

Further, the acid-base equilibria and the thermal stability of the nmyc02 sequence in the pH range 7.1 – 2.5 were characterized. First, acid-base titration of an nmyc02 sample was carried out and CD and molecular absorption spectra were recorded. Selected spectra and the whole data set are shown in Figure 4a-b and Figure S5, respectively. At neutral pH, the CD spectrum of nmyc02 is characterized by a positive band at 265nm and a negative band at 243nm, the intensity of which is approximately half that of the first band. These features are characteristic of a parallel G-quadruplex structure. The absence of a clear shoulder at 295nm rules out the presence of mixed antiparallel/parallel structures [34].

Few changes in the CD spectra were observed upon protonation (Figure 4a), suggesting a stable G-quadruplex structure over the pH range studied. However, a decrease in absorbance at 260 nm and a concomitant increase in absorbance at 280 – 295 nm were observed (Figure 4b). The CD and absorbance data recorded over the acid-base titration of nmyc02 were analyzed using Equispec. The whole set of spectra fitted well when a model involving two acid-base equilibria, i.e., three spectroscopically active species was considered. The pure spectra and the distribution

diagram were thus calculated for this number of species (Figure 4c-e). The pH transition mid-point values were 5.0 ± 0.1 and 3.1 ± 0.2, similar to the pK_a values of free cytosine and adenine, respectively. Accordingly, the acid-base species predominant at pH 7 was related to the G-quadruplex, in which cytosine and adenine bases remained deprotonated. The major species around pH 4.1 was related to the G-quadruplex, in which most of the cytosine bases were protonated whereas most of the adenine bases remained deprotonated. Finally, the structure predominant at pH 2 was related to the G-quadruplex structure, in which all, cytosine and adenine bases, were protonated. Both transitions lack any cooperativity (*p* equal to 1 in Equation 2), a fact that again could be related to the protonation of bases in the loops (i.e., not involved in any base pairing).

As in the case of nmyc01, the nature of the species proposed from the spectroscopically-monitored acid-base titration was also studied using ^{1}H NMR (Supplementary Material, Figure S6, left). At pH 7 and 5^{o}C, the signals at ~11 ppm were related to imino hydrogens in G-quadruplex structures. The broad and unresolved band indicated the existence of multiple conformers in equilibrium, in agreement with the distribution of DNA species observed by PAGE. Confirming the PAGE analysis, the small peaks at 12.8 and 13.5 ppm indicate the existence of Watson-Crick base pairs. At pH 5 and 5^{o}C, all signals were still visible, which indicated the stability of this structure at this pH value. Watson-Crick base pairing in the loop was further evidenced by NMR analysis of the nmyc02 oligonucleotide (Figure S6, right). Indeed, this oligonucleotide did not present at pH 5 or 7 the signal at 13.6 ppm observed with the wild-type sequence, thus showing its inability to stably base-pair the TGCA repeats. The preserved signal around 11 ppm indicated however the conservation of G-quartets, as seen with PAGE.

Further, several melting experiments of nmyc02 samples were performed within the pH range 3.9 – 7.1. Data analysis was similar to that previously described for nmyc01. Figure S7 shows the experimental spectra recorded during a melting at pH 6.1. The trace at 295 nm (inset) was characterized by the low hypochromicity characteristic of G-quadruplex unfolding. As for the unfolding of the *i*-motif structure, the best fits were achieved when two transitions, i.e. three components or conformations, were considered. The first transition was explained initially in terms of a partial unfolding of the nmyc02 G-quadruplex initially present at 20^{o}C and pH 6.1, as the existence of the G-quadruplex structure at 70^{o}C was confirmed by means of CD spectroscopy (data not shown). However, the fact that the magnitude of the first transition, as well as its midpoint, depends on the concentration of DNA (Supplementary Material, Figure S7) points out to the presence of DNA aggregates. The second transition corresponded to the complete unfolding of the G-quadruplex to yield the unordered nmyc02 strand. Table 3

summarizes the thermodynamic values calculated in this way for both transitions. The changes in enthalpy, entropy and Gibbs free energy for the first transition were clearly lower than for the second transition, being related to the differences in abruptness for both transitions. At pH 6.1, the melting temperature (T_m) for the complete unfolding of the G-quadruplex structure was 79 ± 1°C. At this pH, T_m of the second transition was invariant throughout the concentration range 0.8-30 μM, which suggested intramolecular folding in the experimental conditions used in this study. T_m increased concomitantly with a decrease in pH (Table 3 and Figure S3). The increase in T_m value, although not as dramatic as in the case of the nmyc01 sequence, could be due to the effect of pH on the backbone-repulsive interactions that destabilize folded DNA structures, and / or to the formation of additional bonds due to the protonation of cytosine and / or adenine bases in the loops.

From the change in enthalpy corresponding to the second transition it is possible to calculate the number of tetrads present. The formation of G-quadruplex structures is enthalpy driven, with a change in enthalpy per quartet of -15 to -25 kcal/mol [35]. At pH values near 7, the change in enthalpy is around 73 kcal/mol. The change in enthalpy per quartet would be 24 or 18 kcal/mol for a core structure of three or four tetrads, respectively. Table 3 shows that the change in enthalpy corresponding to the second transition increased at pH values lower than approximately 4.5. This could be due to the formation of additional base pairs because of the protonation of cytosine and/or adenine bases in the loops. A similar behavior was observed for the change in entropy. The calculated value for the change in Gibbs free energy at 25°C and pH 7 (10.9 kcal/mol) indicates the high stability of the G-quadruplex under these experimental conditions.

The number of tetrads present in the G-quadruplex structure adopted by nmyc02 was also calculated from the measured ESI-MS spectra (Figure S8). As well as the peaks associated with DNA ions with a definite m/z ratio, several minor peaks related to DNA·NH_4^+ adducts were detected. Hence, the peaks at *m/z* ratios 1807.4 and 1548.8 may be explained when the number of ammonium ions bound equals two (i.e., three tetrads of guanine bases) and the charge *z* is -6 and -7, respectively [36].

Finally, Size-Exclusion Chromatography was used to complement the results obtained from PAGE and the spectroscopic data, the main goal being the confirmation of super-structures of oligonucleotide multimers associated by G-quartets, a common behavior of G-rich oligonucleotides containing multiple stretches of guanines

[27]. Figure 5 shows the chromatograms recorded for a series of samples with increasing concentration. At 1 μM, the chromatogram showed a main peak around 7.4 minutes and a shoulder around 6 minutes. The chromatographic system was calibrated (log MW vs. retention time) with a set of DNA sequences that form linear structures. According to these, the completely linear nmyc02 should elute at 7.1 minutes. The shift from 7.1 to 7.4 minutes can be explained in terms of the formation of a G-quadruplex structure, which has a smaller hydrodynamic volume than the linear structure. When the concentration increased, the Gaussian peak at 7.4 minutes increased accordingly. In addition, the shoulder at 6 minutes increased concomitantly. This was attributed to aggregates that elute earlier than the G-quadruplex due to their larger hydrodynamic volumes. When a sample was incubated for a month at 4^{o}C, the ratio of aggregate increased dramatically (Figure 5b).

Competitive equilibria of Watson-Crick duplex versus intramolecular structures

To plot quantitatively the potential competition between the Watson-Crick duplex and the quadruplex structures formed by nmyc01 and nmyc02, kinetics, acid-base and melting experiments, as well as SEC and ESI-MS measurements involving mixtures of both sequences were carried out.

The kinetics of the formation of the duplex was checked by means of molecular beacons technology using a 5'-fluorescein and 3'-dabsyl-labelled nmyc02 sequence. The maintenance of the G-quadruplex structure in this labeled sequence was checked by means of melting measurements. The determined T_m was 79±1^{o}C, similar to the value for the unlabeled sequence, which confirmed that the structure was not affected by the addition of fluorescein and dabsyl. Upon addition of the stoichiometric amount of the complementary nmyc01 sequence an increase in the fluorescence intensity was observed at 37^{o}C (Figure S9). This was related to the progressive unfolding of the G-quadruplex to yield the Watson-Crick duplex, and subsequent distancing of the fluorophore / quencher pair which enhanced fluorescence. The data fitted a biexponential function with rate constants equal to 0.005±0.002 s^{-1} and 0.0004±0.0001 s^{-1}. This model suggests the existence of two parallel, rather than two consecutive, reactions. The proposed mechanism and the calculated values for the rate constants are in the same order of magnitude as those calculated for the unfolding of a 22-nt human telomere quadruplex in 25mM KCl, 10mM phosphate, pH 7.2 and 20^{o}C [21]. Finally, the formation of the Watson-Crick duplex was completed after incubation at 37^{o}C overnight.

In order to study the formation of the duplex structure throughout a wide pH range, spectroscopically monitored acid-base titrations of nmyc01: nmyc02 mixtures were carried out. As an example, the results obtained after analysis

of a 1:1 nmyc01:nmyc02 mixture are shown here (Figure 6 and S10). Analysis of the experimental data revealed the presence of four spectroscopically active species in the pH range 2.2 – 7.1. The explanation for the proposed acid-base species was not straightforward because some of these actually corresponded to mixtures of two or more of the five different nmyc01 and nmyc02 acid-base species previously described. However, the assignation of the major species at pH 7 to the Watson-Crick duplex was not in doubt. The major species at pH 5 was identified as a mixture of G-quadruplex and *i*-motif structures. The species that appeared at pH values lower than 3 was assigned to a mixture of G-quadruplex and unstructured nmyc01. Finally, the major species at pH 4 was identified as a mixture of G-quadruplex and protonated *i*-motif.

Spectroscopically-monitored melting of a previously incubated 1:1 mixture of nmyc01 and nmyc02 at pH 7.1 yielded a relatively high hyperchromicity at 260nm (around 19% when comparing the absorbance at 95 and 25^{o}C). This fact and the hyperchromicity observed at 295nm revealed the unfolding of a Watson-Crick duplex. The determined T_m (85±1^{o}C) was slightly higher than the value determined for the G-quadruplex (79±1^{o}C). The changes in enthalpy, entropy and Gibbs free energy at 25^{o}C were -254 ± 21 kcal/mol, -683 ± 55 cal/K·mol and -50 ± 5 kcal/mol, respectively. Similar melting experiments were carried out throughout the pH range 4.0 – 7.0 in order to confirm the formation of the duplex (Figure 7). The melting profile at 295 nm recorded for the mixture (1.8 μM of each strand) at pH 6.1 showed two features: a first sharp hypochromic transition around 35^{o}C and a second broad hyperchromic transition around 80^{o}C. The first transition is related to the unfolding of the nmyc01 *i*-motif (T_m = 33^{o}C at this pH value), whereas the second is related to the unfolding of duplex (T_m = 85^{o}C) and of the remaining nmyc02 G-quadruplex (T_m = 79^{o}C). At pH 5.0, there are two transitions (65 and 80^{o}C) that have been related to the unfolding of the *i*-motif and of the G-quadruplex, respectively. As a small amount of hyperchromicity is observed from 73 to 81^{o}C, a minor contribution of the duplex cannot be ruled out, which is in accordance with the proposed distribution diagram (Figure 6).

Figure 8a shows a set of chromatograms recorded for nmyc01, nmyc02 and several mixtures at pH 7.0 and 25^{o}C. The sequence nmyc01 eluted at 7.2 minutes. Upon addition of increasing amounts of nmyc02, the intensity of this peak at 7.2 decreased whereas a new peak appeared around 6.7 minutes. This peak was attributed to the Watson-Crick duplex. This retention time fits perfectly into the calibration plot for linear sequences mentioned above. It should be noted that the peak at 5.6 minutes related to the presence of multimeric structures formed by nmyc02 was not reduced upon formation of the Watson-Crick duplex, and the annealing procedure. Indeed, it is possible that

particularly heat-resistant G-quadruplex structures were not denaturated properly, as suggested by their presence detected even a prolonged incubation at 99^{o}C in presence of KCl (see lane 1 and 5 in Figure 3B). At pH 6.1, however, the addition of nmyc02 to nmyc01 did not produce a high yield of Watson-Crick duplex. Two months later, the peak associated with the duplex (at 6.7 minutes) had clearly increased whereas that associated with the multimers (at 5.8 minutes) had decreased.

Discussion

The study of non-canonical DNA structures is of great interest because of their potential role in some diseases and aging. Concomitantly, the number of G-quadruplex-forming regions observed in the eumetazoa for which complete genomic sequences are available has increased rapidly [37]. Recently, after decades of research *in vitro*, the *in vivo* presence of G-quadruplexes has been proven [16]. On the other hand, the requirement of low pH values for the formation of stable *i*-motif structures seems to be an obstacle for their formation *in vivo*. However, the existence of proteins that specifically bind to cytosine-rich sequences has already been demonstrated [38]. In addition, it has been proposed that the *i*-motifs could form in the presence of crowding agents [39], proteins [4, 40] or even at slightly basic conditions at low temperature and absence of added salt [41]. Under negative supercoiling, the *i*-motif forms under physiological conditions, and in this case it is more likely that stabilizing capping interactions may drive the formation of a favored *i*-motif [8].

In this work, the solution equilibria of two particular cytosine- (nmyc01) and guanine-rich (nmyc02) regions found in the promoter region of the *n-myc* gene were studied. Both sequences, which have not been studied before, contain a duplicate of the TGCA sequence separated by two nucleotides, thus capable of forming a hairpin stabilized by Watson-Crick base pairs. The cytosine-rich sequence forms two intramolecular *i*-motifs that are stable throughout the pH range 2 - 7, with maximal stability at pH 4.5. Under physiological conditions of pH and temperature, the relative concentration of the *i*-motif structure is small. The difference between the two *i*-motifs depends on the protonation of additional bases in the loops. Our results also show that the guanine-rich region forms an intramolecular parallel G-quadruplex that is stable throughout the studied pH range (2 - 7). Finally, the competition between the intramolecular structures (G-quadruplex and *i*-motif) and the intermolecular Watson-Crick duplex formed was studied, revealing that the Watson-Crick duplex is the predominant form at pH values above 6. Figure 9

depicts a schematic view of the two proposed intramolecular structures. The precise determination of the three-dimensional solution structure of all sequences studied here is beyond the scope of this manuscript.

The sequences studied here actually correspond to the wild-type sequences, and contain cytosine and guanine tracts of unequal length. They are thus expected to form potentially multiple conformers that could interconvert at temperatures below T_m, as has been observed for *i*-motif structures formed within the HIF-1α proximal promoter [42]. This could explain the broad NMR signals observed for the *i*-motif and G-quadruplex. Accurate determination of the solution structures will require the systematic mutation of bases located in these tracts in order to reduce the conformational space sampled by the wild-type sequences.

The existence of two different *i*-motif structures, which mainly differ according to the protonation of bases in the loops, was previously proposed for a cytosine-rich sequence in the promoter region of the *bcl-2* gene [5]. As in this previous work, the current study demonstrated the utility of a multivariate approach to extract quantitative information (distribution diagram) from the measured CD and molecular absorption spectra. Monitoring a process such as acid-base titration at just one wavelength clearly leads to the loss of valuable information.

The most striking characteristic of both quadruplex structures is the existence of a long loop that incorporates a short stretch of Watson-Crick base pairs. To our knowledge, no previous report has been published describing any *i*-motif structure with such a long hairpin loop. In a recent article, Brazier *et al.* reported the extraordinary stability of a cytosine-rich region in the PDGF-A gene which contains six tracts of cytosine numbering from 2 to 13 bases long [42]. This stability, however, was explained there in terms of long cytosine-rich loop regions, rather than by the formation of intramolecular hairpins. In our case, the existence of this loop stabilizes the structure in terms of ΔH^0, ΔS^0 and ΔG^0. However, this stabilization is not directly related to an increase in the melting temperature. The argument that an increase in T_m can be directly related to an increase in stability at a given temperature has previously been debated [43, 44]. Obviously, at 25°C and pH 5.0, both structures are folded. However, the unfolding of the wild-type sequence (nmyc01) is completed over a narrower temperature range than that of the mutated sequence (nmyc01m). As a consequence, the structure involving the Watson-Crick stem inside the long loop has a higher stability at 25°C and pH 5.0 than the structure without that stem. This suggests the contribution of the hairpin to the stability of the overall structure, and our PAGE analysis suggest that this hairpin stabilizes one particular motif to favor the intramolecular folding of n-myc01 and/or n-myc02, and consequentially decreases intermolecular

interactions giving rise to DNA multimers of high molecular weight, widely reported in the field of G-quadruplex forming structures. This behavior is particularly interesting in a biological context where formation of this stem-loop, repeated on both strand, could greatly contribute to the folding of both i- and G tetraplexes upon local unwinding of the nmyc promoter.

The data on the thermal stability of *i*-motifs has led to the proposal of two classes (I and II) into which currently known *i*-motifs can be grouped. Class I structures consist of short loop regions between cytosine tracts, whereas class II structures contain longer loop regions between cytosine tracts [18]. The classification of the *i*-motif formed by nmyc01 points to an intermediate situation between these two classes. The transitional pH from the single strand is 6.5, which classifies it as a class II *i*-motif. However, the thermal stability at pH 7 and the proposed short loops 2 and 3 indicate that it is a class I *i*-motif.

The reported data on the stability of G-quadruplexes show that, in general, the most stable in terms of T_m values are those containing single-nucleotide lateral loops between the G-quartets [45]. The G-quadruplex structure that could be formed by the n-myc02 sequence contains at least one such loop. In addition, the presence of two single-nucleotide loops within a quadruplex-forming sequence constrains the structure to a parallel fold, which is independent of the length of the remaining loop (up to three nucleotides) [45]. In the case of nmyc02, the presence of a longer loop does not prevent the formation of a parallel G-quadruplex, as shown by CD spectroscopy. As the opposite, the formation of a short stem-loop greatly stabilizes a single, monodisperse structure as seen with gel electrophoresis. Other wild-type guanine-rich sequences, like those corresponding to the hypoxia inducible factor 1α promoter [46] and c-myc [47], also show parallel folding despite containing relatively long loops. Concerning the formation of a hairpin, to our knowledge only one parallel G-quadruplex structure containing a hairpin in a loop has been described previously, being that found at the hTERT core promoter [48]. As in the case of nmyc02, the long loop likely forms a stable hairpin structure, which would explain the unexpected stability of both G-quadruplex structures.

The first transition observed in the melting of nmyc02 was explained initially in terms of partial unfolding of the nmyc02 G-quadruplex initially present at 20^{o}C and pH 6.1. This transition would involve some unstacking of bases located in the loops or at the 5’ or 3’ ends of the nmyc02 sequence. However, in view of the SEC results, the first transition could be related to the breaking of the aggregates at temperatures lower than the melting temperature.

The formation of multimers has been proposed for other sequences [49], including a sequence lacking of a long loop in the n-myc gene (5'-$TAG_3CG_3AG_3AG_3A_2$-3'), [22]. In this last work, the melting of the dimeric form was not reflected in temperature-dependent UV absorbance profiles. Again, the application of a multivariate approach allowed the resolution of a complete distribution diagram for the unfolding of a complex mixture. Finally, the presence of multimers for the nmyc02 sequence is consistent with the observation that two parallel processes occur during the formation of the Watson-Crick duplex from the folded G-quadruplex, as indicated by the fluorescence and SEC measurements.

This work has also shown that the Watson-Crick duplex is the predominant species in the mixture at pH 7 and 25^{o}C. However, low numbers of intramolecular structures are present at this pH, their contribution being higher than that of the duplex at pH values lower than approximately 6.1. The pH value is, as a consequence, a key variable modulating the equilibrium between the intra- and intermolecular species. Dysregulated pH is known to be an adaptive feature of most cancers, regardless of their tissue origin or genetic background. In normal differentiated adult cells, intracellular pH is generally lower (around 7.2) than the extracellular pH (around 7.4). However, cancer cells have a higher intracellular (around 7.4) and a lower extracellular pH (6.7–7.1) [50]. In these conditions, cytosine-rich sequences may adopt *i*-motif structures and modulate the formation of the other nucleic acid structures.

Acknowledgements

Thanks are due to Robert Hänsel (Goethe University Frankfurt) for helpful discussions about the stability of *i*-motifs. We acknowledge funding from the Spanish government (CTQ2012-38616-C02-02 and CTQ2010-20541-C03-01).

Bibliography

[1] S. Ahmed, A. Kintanar, E. Henderson, Human Telomeric C-Strand Tetraplexes, Nature Structural Biology, 1 (1994) 83-88.

[2] J.L. Leroy, M. Gueron, J.L. Mergny, C. Helene, Intramolecular Folding of a Fragment of the Cytosine-Rich Strand of Telomeric DNA into an I-Motif, Nucleic Acids Research, 22 (1994) 1600-1606.

[3] S. Nonin-Lecomte, J.L. Leroy, Structure of a C-rich strand fragment of the human centromeric satellite III: A pH-dependent intercalation topology, Journal of Molecular Biology, 309 (2001) 491-506.

[4] D.J. Uribe, K. Guo, Y.-J. Shin, D. Sun, Heterogeneous Nuclear Ribonucleoprotein K and Nucleolin as Transcriptional Activators of the Vascular Endothelial Growth Factor Promoter through Interaction with Secondary DNA Structures, Biochemistry, 50 (2011) 3796-3806.

[5] N. Khan, A. Avino, R. Tauler, C. Gonzalez, R. Eritja, R. Gargallo, Solution equilibria of the i-motif-forming region upstream of the B-cell lymphoma-2 P1 promoter, Biochimie, 89 (2007) 1562-1572.

[6] G. Manzini, N. Yathindra, L.E. Xodo, Evidence for Intramolecularly Folded I-DNA Structures in Biologically Relevant Ccc-Repeat Sequences, Nucleic Acids Research, 22 (1994) 4634-4640.

[7] K. Guo, A. Pourpak, K. Beetz-Rogers, V. Gokhale, D. Sun, L.H. Hurley, Formation of Pseudosymmetrical G-Quadruplex and i-Motif Structures in the Proximal Promoter Region of the RET Oncogene, J. Am. Chem. Soc., 129 (2007) 10220-10228.

[8] D. Sun, L.H. Hurley, The Importance of Negative Superhelicity in Inducing the Formation of G-Quadruplex and i-Motif Structures in the c-Myc Promoter: Implications for Drug Targeting and Control of Gene Expression, Journal of Medicinal Chemistry, 52 (2009) 2863-2874.

[9] S. Saxena, A. Bansal, S. Kukreti, Structural polymorphism exhibited by a homopurine·homopyrimidine sequence found at the right end of human c-jun protooncogene, Archives of Biochemistry and Biophysics, 471 (2008) 95-108.

[10] Y. Xu, H. Sugiyama, Formation of the G-quadruplex and i-motif structures in retinoblastoma susceptibility genes (Rb), Nucleic Acids Research, 34 (2006) 949-954.

[11] Y. Peng, X. Wang, Y. Xiao, L. Feng, C. Zhao, J. Ren, X. Qu, i-Motif Quadruplex DNA-Based Biosensor for Distinguishing Single- and Multiwalled Carbon Nanotubes, Journal of the American Chemical Society, 131 (2009) 13813-13818.

[12] P. Alberti, A. Bourdoncle, B. Sacca, L. Lacroix, J.L. Mergny, DNA nanomachines and nanostructures involving quadruplexes, Organic & Biomolecular Chemistry, 4 (2006) 3383-3391.

[13] S. Neidle, Human telomeric G-quadruplex: The current status of telomeric G-quadruplexes as therapeutic targets in human cancer, FEBS Journal, 277 (2010) 1118-1125.

[14] J.L. Huppert, Quadruplexes in the Genome, in: S. Neidle, S. Balasubramanian (Eds.) Quadruplex Nucleic Acids, The Royal Society of Chemistry, Cambridge, 2006, pp. 208-223.

[15] J.L. Huppert, Structure, location and interactions of G-quadruplexes, FEBS Journal, 277 (2010) 3452-3458.

[16] G. Biffi, D. Tannahill, J. McCafferty, S. Balasubramanian, Quantitative visualization of DNA G-quadruplex structures in human cells, Nat Chem, advance online publication (2013).

[17] S. Balasubramanian, S. Neidle, G-quadruplex nucleic acids as therapeutic targets, Current Opinion in Chemical Biology, 13 (2009) 345-353.

[18] T.A. Brooks, S. Kendrick, L. Hurley, Making sense of G-quadruplex and i-motif functions in oncogene promoters, FEBS Journal, 277 (2010) 3459-3469.

[19] P. Bucek, J. Jaumot, A. Avino, R. Eritja, R. Gargallo, PH-modulated Watson-Crick duplex-quadruplex equilibria of guanine-rich and cytosine-rich DNA sequences 140 base pairs upstream of the c-kit transcription initiation site, Chemistry - A European Journal, 15 (2009) 12663-12671.

[20] E. Bell, L. Chen, T. Liu, G.M. Marshall, J. Lunec, D.A. Tweddle, MYCN oncoprotein targets and their therapeutic potential, Cancer Letters, 293 (2010) 144-157.

[21] A.N. Lane, The stability of intramolecular DNA G-quadruplexes compared with other macromolecules, Biochimie, 94 (2012) 277-286.

[22] M. Trajkovski, M. Webba da Silva, J. Plavec, Unique Structural Features of Interconverting Monomeric and Dimeric G-Quadruplexes Adopted by a Sequence from the Intron of the N-myc Gene, Journal of the American Chemical Society, 134 (2012) 4132-4141.

[23] D.M. Tasset, M.F. Kubik, W. Steiner, Oligonucleotide inhibitors of human thrombin that bind distinct epitopes, Journal of Molecular Biology, 272 (1997) 688-698.

[24] J. Jaumot, R. Gargallo, Experimental methods for studying the interactions between G-quadruplex structures and ligands, Current Pharmaceutical Design, 18 (2012) 1900-1916.
[25] W.A. Kibbe, OligoCalc: An online oligonucleotide properties calculator, Nucleic Acids Research, 35 (2007) W43-W46.
[26] M. Piotto, V. Saudek, V. Sklenár, Gradient-tailored excitation for single-quantum NMR spectroscopy of aqueous solutions, Journal of Biomolecular NMR, 2 (1992) 661-665.
[27] S. Ruiz-Castelar, A. Checa, R. Gargallo, J. Jaumot, Combination of chromatographic and chemometric methods to study the interactions between DNA strands, Analytica Chimica Acta, 722 (2012) 34-42.
[28] J. Jaumot, R. Eritja, R. Gargallo, Chemical equilibria studies using multivariate analysis methods, Analytical and Bioanalytical Chemistry, 399 (2011) 1983-1997.
[29] R. Dyson, S. Kaderli, G.A. Lawrence, M. Maeder, A.D. Zuberbühler, Second order global analysis: the evaluation of series of spectrophotometric titrations for improved determination of equilibrium constants, Analytica Chimica Acta, 353 (1997) 381-393.
[30] S. Fernandez, R. Eritja, A. Aviñó, J. Jaumot, R. Gargallo, Influence of pH, temperature and the cationic porphyrin TMPyP4 on the stability of the i-motif formed by the 5'-(C3TA2)4-3' sequence of the human telomere, International Journal of Biological Macromolecules, 49 (2011) 729-736.
[31] J.L. Mergny, L. Lacroix, X.G. Han, J.L. Leroy, C. Helene, Intramolecular Folding of Pyrimidine Oligodeoxynucleotides into an I-DNA Motif, Journal of the American Chemical Society, 117 (1995) 8887-8898.
[32] T. Vojtylová, D. Dospivová, O. Trisková, I. Pilarová, P. Lubal, M. Farková, L. Trnková, P. Táborský, Spectroscopic study of protonation of oligonucleotides containing adenine and cytosine, Chemical Papers, 63 (2009) 731-737.
[33] M. Adrian, B. Heddi, A.T. Phan, NMR spectroscopy of G-quadruplexes, Methods, 57 (2012) 11-24.
[34] G.N. Parkinson, Fundamentals of Quadruplex Structures, in: S. Neidle, S. Balasubramanian (Eds.) Quadruplex Nucleic Acids, The Royal Society of Chemistry, Cambridge, 2006, pp. 1-30.
[35] J.-L. Mergny, J. Gros, A.D. Cian, A. Bourdoncle, F. Rosu, B. Saccà, L. Guittat, S. Amrane, M. Mills, P. Alberti, M. Takasugi, L. Lacrois, Energetics, Kinetics and Dynamics of Quadruplex Folding, in: S. Neidle, S. Balasubramanian (Eds.) Quadruplex Nucleic Acids, The Royal Society of Chemistry, Cambridge, 2006, pp. 31-72.
[36] F. Rosu, V. Gabelica, C. Houssier, P. Colson, E. De Pauw, Triplex and quadruplex DNA structures studied by electrospray mass spectrometry, Rapid Communications in Mass Spectrometry, 16 (2002) 1729-1736.
[37] S.S. Smith, Evolutionary Expansion of Structurally Complex DNA Sequences, Cancer Genomics - Proteomics, 7 (2010) 207-215.
[38] Y.M.K. Yoga, D.A.K. Traore, M. Sidiqi, C. Szeto, N.R. Pendini, A. Barker, P.J. Leedman, J.A. Wilce, M.C.J. Wilce, Contribution of the first K-homology domain of poly(C)-binding protein 1 to its affinity and specificity for C-rich oligonucleotides, Nucleic Acids Research, 40 (2012) 5101-5114.
[39] D. Miyoshi, S. Matsumura, S.I. Nakano, N. Sugimoto, Duplex Dissociation of Telomere DNAs Induced by Molecular Crowding, Journal of the American Chemical Society, 126 (2004) 165-169.
[40] A. Bandiera, G. Tell, E. Marsich, A. Scaloni, G. Pocsfalvi, A. Akindahunsi, L. Cesaratto, G. Manzini, Cytosine-block telomeric type DNA-binding activity of hnRNP proteins from human cell lines, Archives of Biochemistry and Biophysics, 409 (2003) 305-314.
[41] J. Zhou, C. Wei, G. Jia, X. Wang, Z. Feng, C. Li, Formation of i-motif structure at neutral and slightly alkaline pH, Molecular BioSystems, 6 (2010) 580-586.
[42] J.A. Brazier, A. Shah, G.D. Brown, I-Motif formation in gene promoters: unusually stable formation in sequences complementary to known G-quadruplexes, Chemical Communications, 48 (2012) 10739-10741.
[43] L.A. Marky, K.J. Breslauer, Calculating thermodynamic data for transitions of any molecularity from equilibrium melting curves, Biopolymers - Peptide Science Section, 26 (1987) 1601-1620.
[44] J.L. Mergny, L. Lacroix, Analysis of Thermal Melting Curves, Oligonucleotides, 13 (2003) 515-537.
[45] A. Bugaut, S. Balasubramanian, A Sequence-Independent Study of the Influence of Short Loop Lengths on the Stability and Topology of Intramolecular DNA G-Quadruplexes Biochemistry, 47 (2008) 689-697.
[46] R. De Armond, S. Wood, D. Sun, L.H. Hurley, S.W. Ebbinghaus, Evidence for the presence of a guanine quadruplex forming region within a polypurine tract of the hypoxia inducible factor 1-alfa promoter, Biochemistry, 44 (2005) 16341-16350.
[47] A.T. Phan, Y.S. Modi, D.J. Patel, Propeller-type parallel-stranded G-quadruplexes in the human c-myc promoter, Journal of the American Chemical Society, 126 (2004) 8710-8716.
[48] S.L. Palumbo, S.W. Ebbinghaus, L.H. Hurley, Formation of a Unique End-to-End Stacked Pair of G-Quadruplexes in the hTERT Core Promoter with Implications for Inhibition of Telomerase by G-Quadruplex-Interactive Ligands, Journal of the American Chemical Society, 131 (2009) 10878-10891.

[49] N. Smargiasso, F. Rosu, W. Hsia, P. Colson, E.S. Baker, M.T. Bowers, E. De Pauw, V. Gabelica, G-quadruplex DNA assemblies: Loop length, cation identity, and multimer formation, Journal of the American Chemical Society, 130 (2008) 10208-10216.
[50] B.A. Webb, M. Chimenti, M.P. Jacobson, D.L. Barber, Dysregulated pH: a perfect storm for cancer progression, Nat Rev Cancer, 11 (2011) 671-677.

Tables and figures

Table 1. Sequences studied in this work. Underlined bases are those that could be involved in the formation of C+•C base pairs or guanine tetrads. F and Q denote fluorophore and quencher, respectively.

Table 2. Thermodynamic parameters for the unfolding of nmyc01 and nmyc01m calculated from melting experiments. The experiments were carried out in 20 mM phosphate or acetate buffer, 150 mM KCl, 1.3 μM nmyc01 or nmyc01m.

Table 3. Thermodynamic parameters for the unfolding of nmyc02 calculated from melting experiments. T_m values are given in °C. ΔH^0 and ΔG^0 values (at 25°C) are given in kcal·mol^{-1}. ΔS^0 is given in cal·K^{-1}·mol^{-1}. Experiments were carried out in 20 mM phosphate or acetate buffer, 150 mM KCl, 1.6 μM nmyc02.

Figure 1. Acid-base titration of an nmyc01 sample monitored with CD and molecular absorption spectroscopy. (a) Selected set of CD experimental spectra. Inset: pH values at which the spectra were measured. (b) Selected set of molecular absorption spectra. (c) Calculated distribution diagram. (d) Calculated CD spectra. (e) Calculated molecular absorption spectra. Blue line: neutral form, probably a partially stacked single strand; red line: *i*-motif 1; green line: *i*-motif 2; black line: protonated form, probably a random coil. C_{nmyc01} = 1.3 μM, T = 25°C.

Figure 2. 600-MHz ^{1}H NMR spectra of the exchangeable imino region of nmyc01 (left) and nmyc01m (right) at pH 7.0, 5.0 and 3.9. All spectra were measured in 100 mM KCl, 25 mM disodium phosphate, 5°C, C_{DNA} = 0.58 mM.

Figure 3. Separation of DNA species for nmyc01 (A) and nmyc02 (B) by non denaturing PAGE buffered at pH 5.2 (left panel) and pH 8 (right panel). The dry oligonucleotides nmyc01 and nmyc01m were suspended at C_{DNA}= 17μM in a 20mM Sodium Acetate (pH 5.2) buffer containing 150mM KCl, the oligonucleotides nymc02 and nmyc02m suspended in a 20mM Tris Acetate (pH 7.2) buffer containing 150mM KCl. The oligonucleotides were heated at 95°C for 10 minutes, cooled down to room temperature overnight and stored two days at +4°C. Immediately before loading, the oligonucleotides were diluted 1/10 in their respective buffers and half of the volume was incubated for 15 minutes at 99°C and chilled on ice (noted as D) whereas the other volume was kept on ice (noted as N). Half of each solution was loaded on both gels that migrated concomitantly. U indicates the band on the unstructured monomer, the arrows point the major retarded band obtain with nmyc01 and nmyc02. Asterisks in (A) indicate the probable multimeric species assembled from nmyc01m in lane 3.

Figure 4. Acid-base titration of an nmyc02 sample monitored with CD and molecular absorption spectroscopy. (a) Selected set of CD experimental spectra. Inset: pH values at which the spectra were measured. (b) Selected set of molecular absorption spectra. (c) Calculated distribution diagram. (d) Calculated CD spectra. (e) Calculated molecular absorption spectra. Blue line: G-quadruplex containing all bases in their neutral forms. Red line: G-quadruplex containing protonated cytosine bases. Green line: G-quadruplex containing protonated cytosine and adenine bases. C_{nmyc02} = 0.9 μM, T = 25°C. Other conditions are as detailed in the text.

Figure 5. SEC of nmyc02 sequence**.** Chromatograms at 260nm recorded for different concentrations of nmyc02 (a) and chromatogram measured for a 1 μM sample kept at 4°C for one month after preparation. The mobile phase was 75mM potassium phosphate adjusted to pH 7.2, and the temperature was 25°C.

Figure 6. Titration of a 1:1 nmyc01:nmyc02 sample monitored with CD and molecular absorption spectroscopy. The results were obtained after analysis of experimental spectra with Equispec. (a) Calculated distribution diagram; (b) Calculated CD spectra; (c) Calculated molecular absorption spectra. Blue line: Watson-Crick duplex, red line: G-quadruplex + i-motif 1, green line: G-quadruplex + i-motif 2, black line: G-quadruplex + unfolded nmyc01. C_{nmyc01} = C_{nmyc02} = 2.0 μM, T = 25°C. Other experimental conditions are as described in the text.

Figure 7. Melting of equimolar mixtures at pH 7.1 (solid line), pH 6.1 (dashed line) and 5.0 (dotted line). The concentration of each strand was 1.8 μM. Other experimental conditions are as described in the text.

Figure 8. Recorded SEC chromatograms for equimolar mixtures of nmyc01 and nmyc02 at pH 7.0 (a) and at pH 6.0 (b and c). The chromatograms shown in c) were recorded two months after the preparation of the mixtures. The mobile phase was 75mM potassium phosphate adjusted to the considered pH value. T= 25°C. The legend shows the nmyc01:nmyc02 ratio of concentrations in each chromatogram.

Figure 9. Proposed schematic structures for the *i*-motif and G-quadruplex structures formed by the nmyc01 and nmyc02 sequences, respectively, under the experimental conditions used in this work.

Table 1. Sequences studied in this work. Underlined bases are those that could be involved in the formation of C^+·C base pairs or guanine tetrads. Bold bases are those mutated to prevent the formation of Watson-Crick base pairing. F and Q denote fluorophore and quencher, respectively.

	Sequence
nmyc01	5′-ACC CCC TGC ATC TGC ATG CCC CCT CCC ACC CCC T-3′
nmyc01m	5′-ACC CCC TGC ATC T**TT** **T**TG CCC CCT CCC ACC CCC T-3′
nmyc02	5′-AGG GGG TGG GAG GGG GCA TGC AGA TGC AGG GGG T-3′
nmyc02m	5' AGG GGG TGG GAG GGG GC**T** T**TT** **T**GA TGC AGG GGG T 3'
Fnmyc02Q	5′-F- AGG GGG TGG GAG GGG GCA TGC AGA TGC AGG GGG T-Q-3′

Table 2. Thermodynamic parameters for the unfolding of nmyc01 and nmyc01m calculated from melting experiments. The experiments were carried out in 20 mM phosphate or acetate buffer, 150 mM KCl, 1.3 μM nmyc01 or nmyc01m.

pH	DNA	Tm (^{o}C)	ΔH^0 (kcal/mol)	ΔS^0 (cal/K·mol)	ΔG^0_{25oC} (kcal/mol)
3.7	nmyc01	62	60	179	6.6
4.5	nmyc01	70	78	228	10.0
5.0	nmyc01	63	83	248	9.1
5.5	nmyc01	50	73	225	5.9
5.8	nmyc01	41	57	179	3.6
6.1	nmyc01	33	52	170	1.2
6.4	nmyc01	25	59	197	0.3
7.0	nmyc01	<15	Not calculated	Not calculated	Not calculated
5.0	nmyc01m	61	69	206	7.6
6.1	nmyc01m	33	43	141	1.0

[a] T_m values are given with an uncertainty value of ± 1^{o}C.

[b] Estimated uncertainty values for thermodynamic data are 10% (ΔG^0) and 5% (ΔH^0 and ΔS^0).

Table 3. Thermodynamic parameters for the unfolding of nmyc02 calculated from melting experiments. T_m values are given in ^oC. ΔH^0 and ΔG^0 values (at 25^oC) are given in kcal·mol^{-1}. ΔS^0 is given in cal·K^{-1}·mol^{-1}. Experiments were carried out in 20 mM phosphate or acetate buffer, 150 mM KCl, 1.6 μM nmyc02.

pH	First transition			Second transition			
	ΔH^0 (kcal/mol)	ΔS^0 (cal/K·mol)	$\Delta G^0_{25^\circ C}$ (kcal/mol)	ΔH^0 (kcal/mol)	ΔS^0 (cal/K·mol)	$\Delta G^0_{25^\circ C}$ (kcal/mol)	T_m (˚C)
3.9	34	103	3.4	114	313	20.7	89
4.5	30	96	1.3	85	236	14.4	86
5.1	34	105	2.8	73	207	11.4	80
6.1	23	73	1.2	74	209	11.2	79
7.1	20	65	1.1	73	209	10.9	77

[a] T_m values are given with an uncertainty value of ± 1^oC.

[b] Estimated uncertainty values for thermodynamic data are 10% (ΔG^0) and 5% (ΔH^0 and ΔS^0).

Figure 1

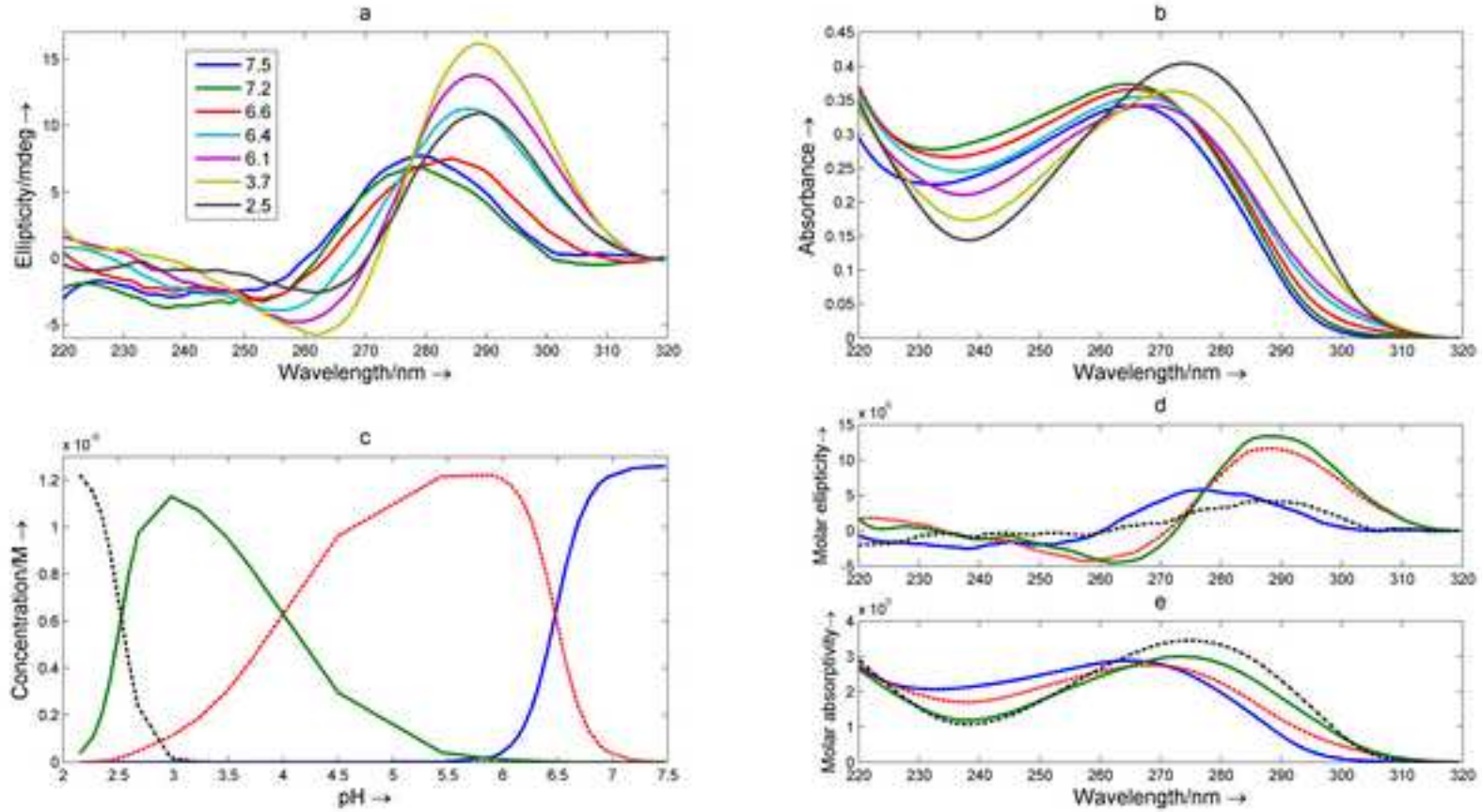
a
Ellipticity/mdeg →
Wavelength/nm →
7.5
7.2
6.6
6.4
6.1
3.7
2.5
b
Absorbance →
Wavelength/nm →
c
Concentration/M →
pH →
d
Molar ellipticity →
e
Molar absorptivity →
Wavelength/nm →

Figure 2

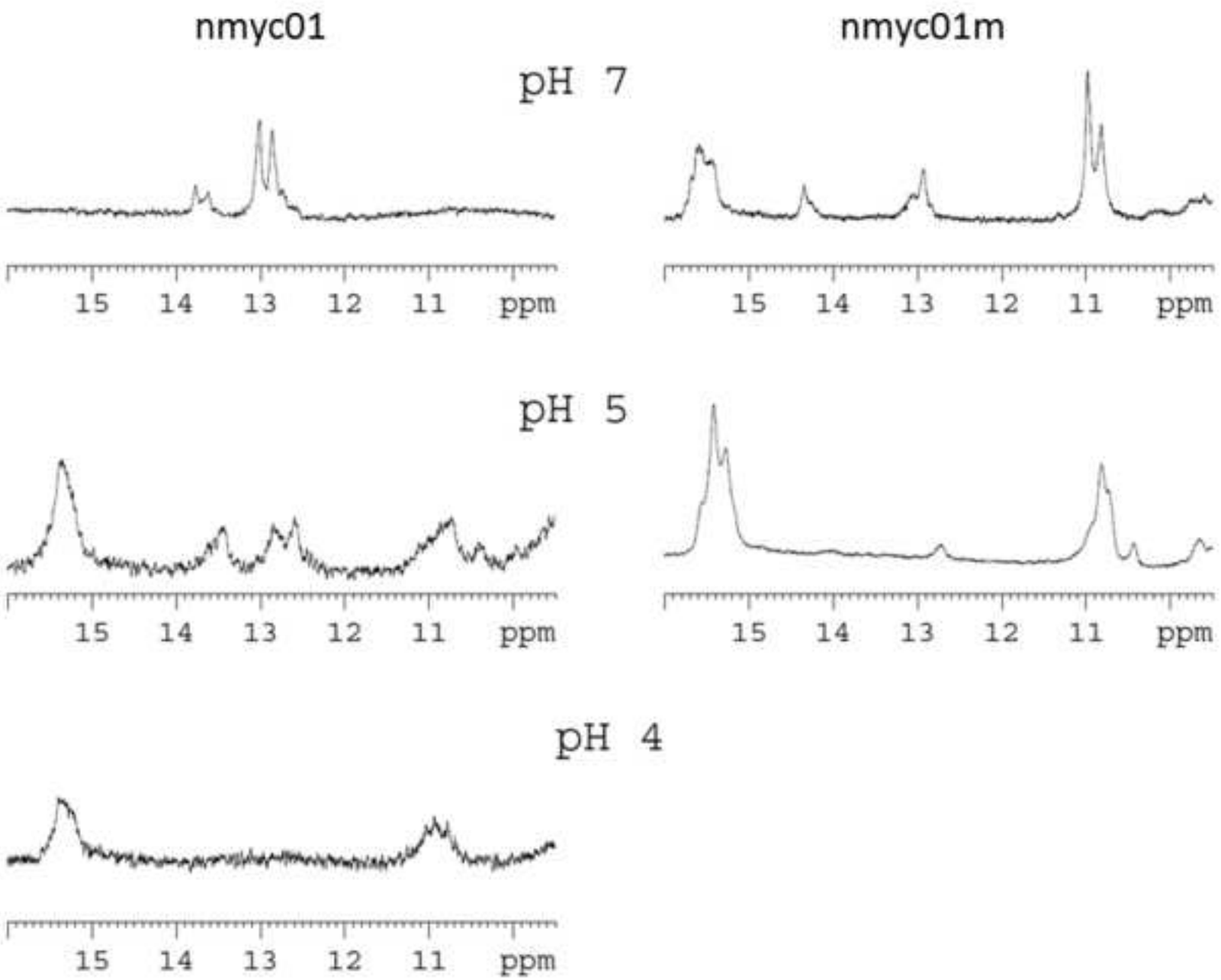

Figure 3

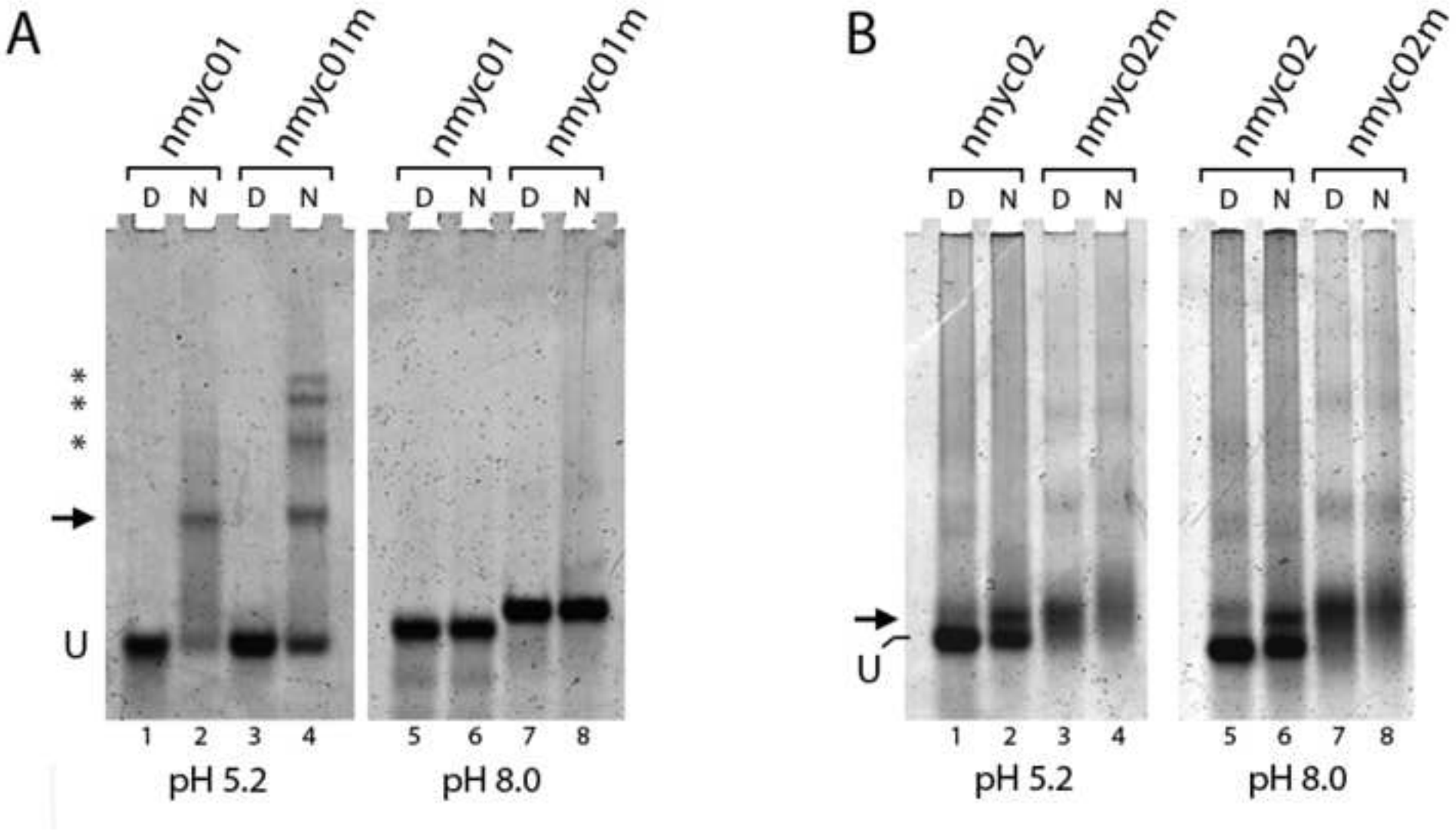
A
nmyc01
nmyc01m
nmyc01
nmyc01m
D N D N D N D N
*
*
*
U
1 2 3 4 5 6 7 8
pH 5.2
pH 8.0
B
nmyc02
nmyc02m
nmyc02
nmyc02m
D N D N D N D N
U
1 2 3 4 5 6 7 8
pH 5.2
pH 8.0

Figure 4

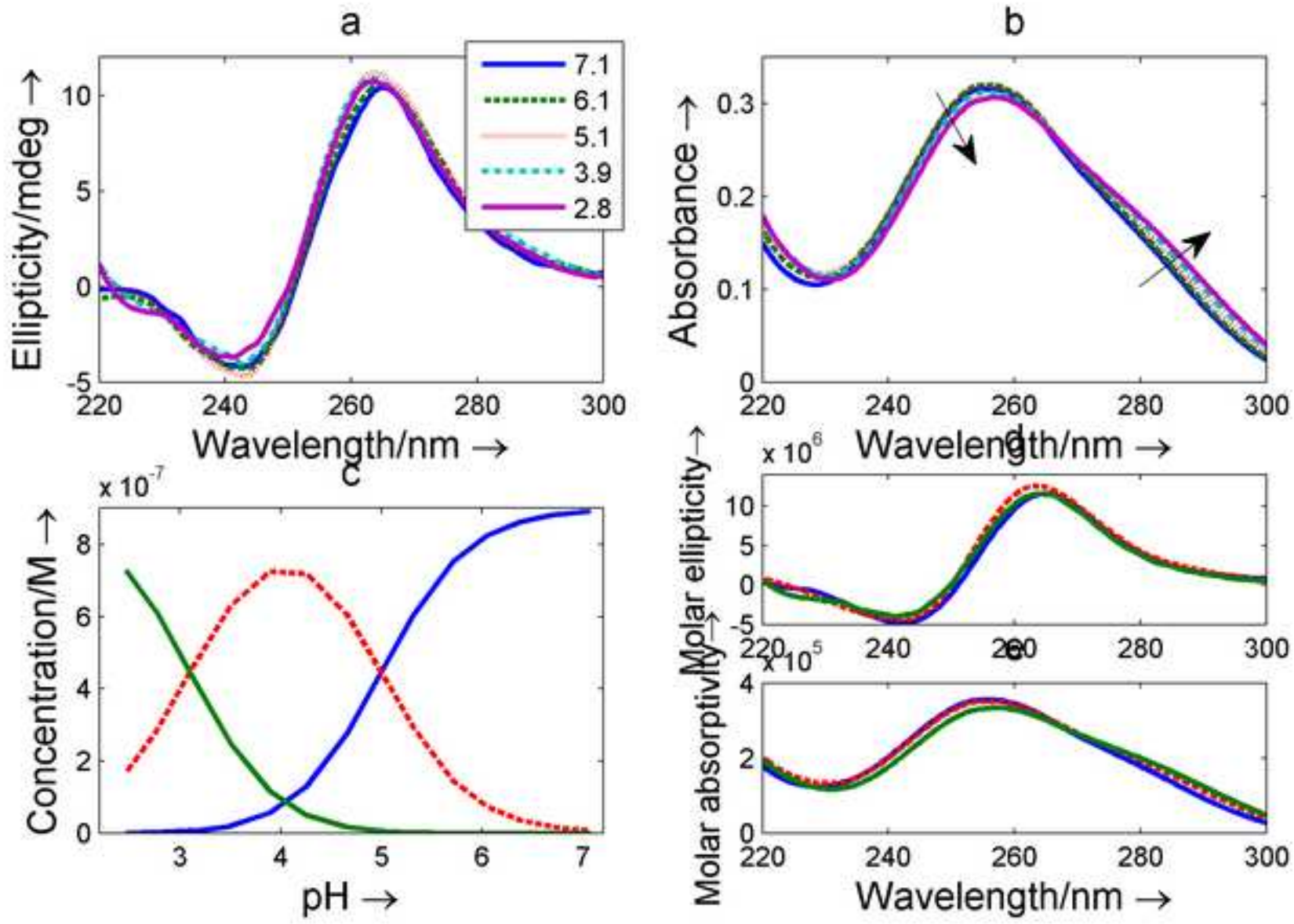
a
Ellipticity/mdeg →
Wavelength/nm →
7.1
6.1
5.1
3.9
2.8
b
Absorbance →
Wavelength/nm →
c
x 10^-7
Concentration/M →
pH →
d
x 10^6
Molar ellipticity →
e
x 10^5
Molar absorptivity →
Wavelength/nm →

Figure 5

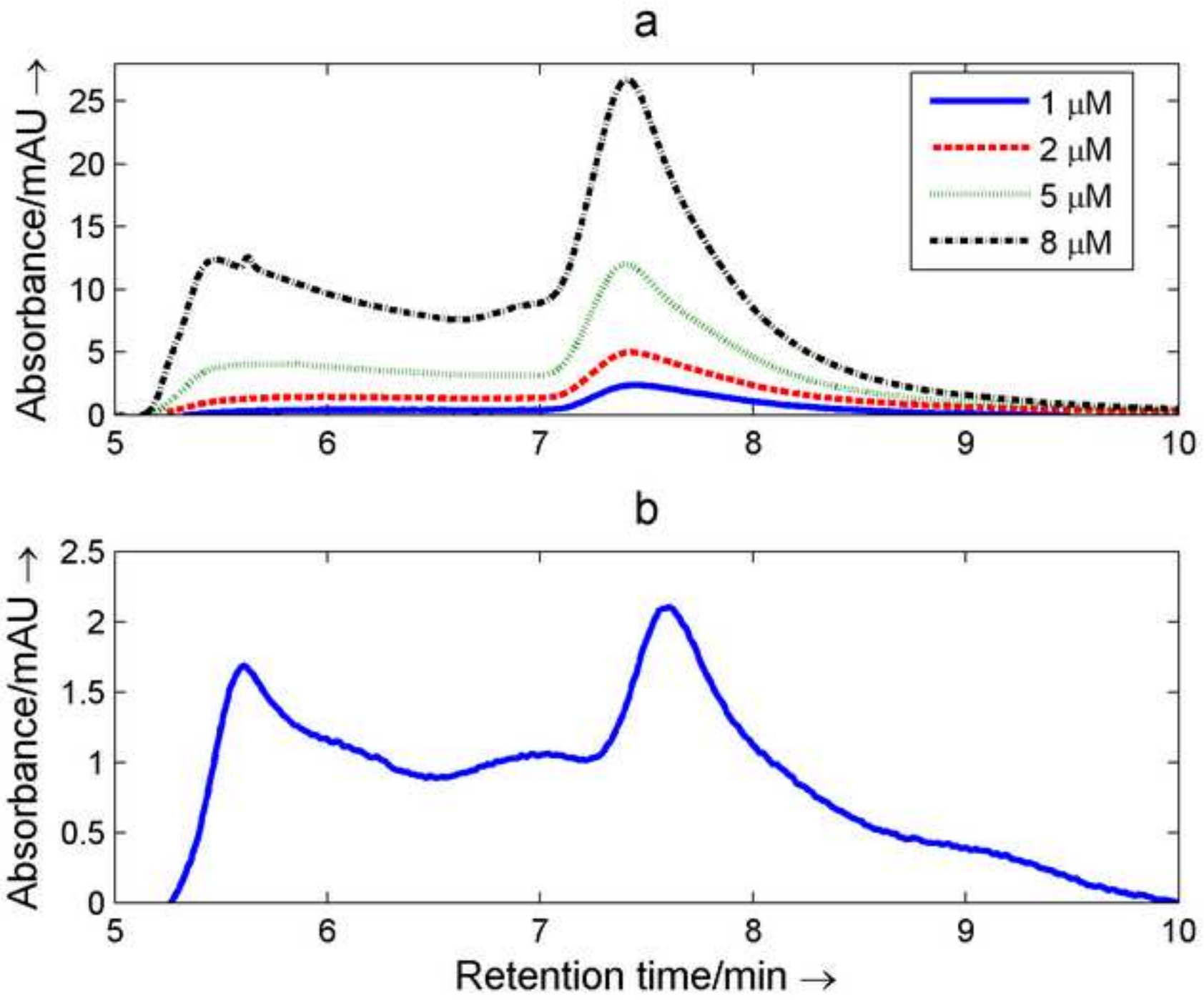
a
Absorbance/mAU →
25
20
15
10
5
0
5
6
7
8
9
10
1 μM
2 μM
5 μM
8 μM
b
Absorbance/mAU →
2.5
2
1.5
1
0.5
0
5
6
7
8
9
10
Retention time/min →

Figure 6

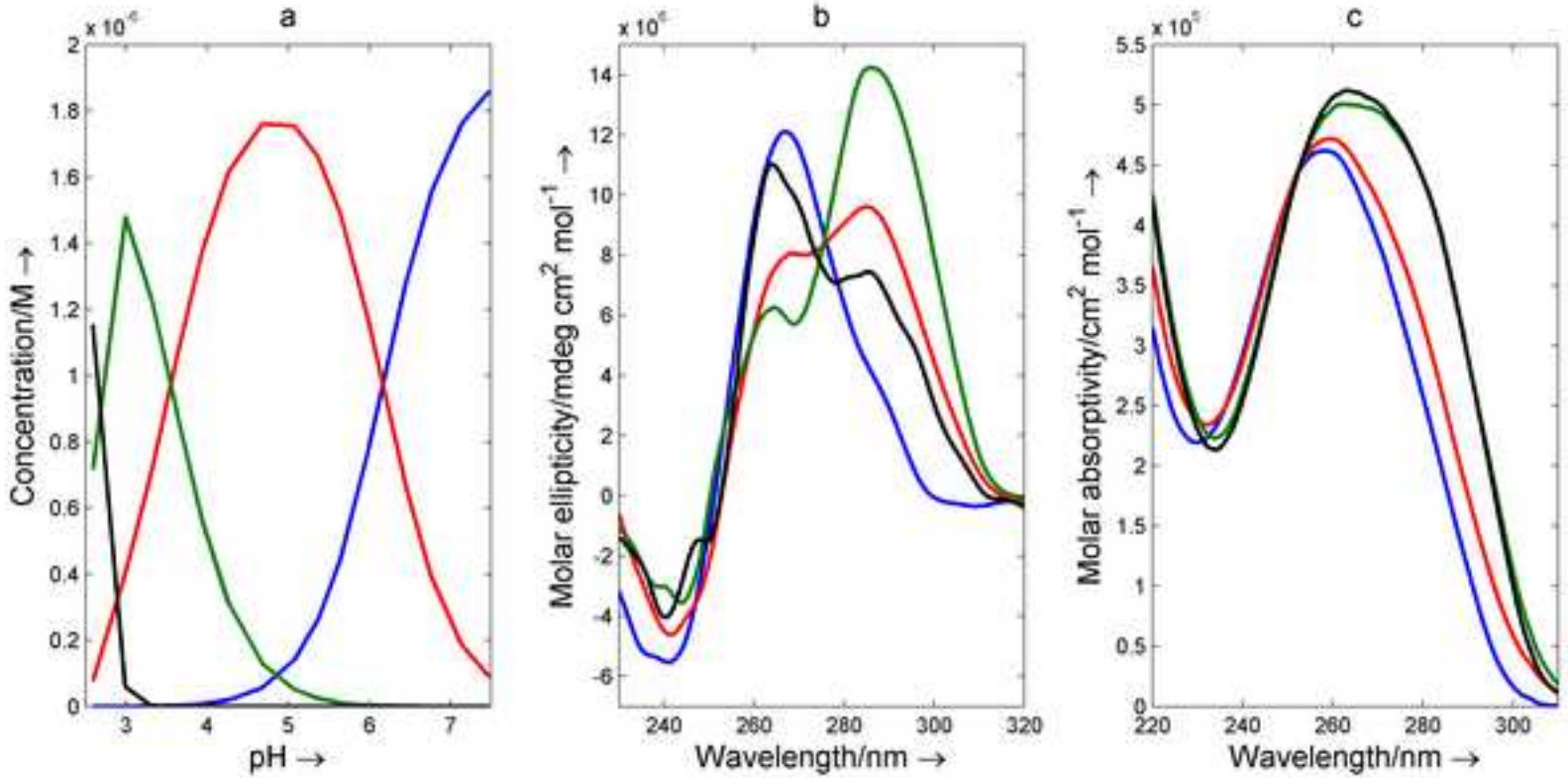
a
x 10^-5
Concentration/M →
pH →
b
x 10^5
Molar ellipticity/mdeg cm^2 mol^-1 →
Wavelength/nm →
c
x 10^5
Molar absorptivity/cm^2 mol^-1 →
Wavelength/nm →

Figure 7

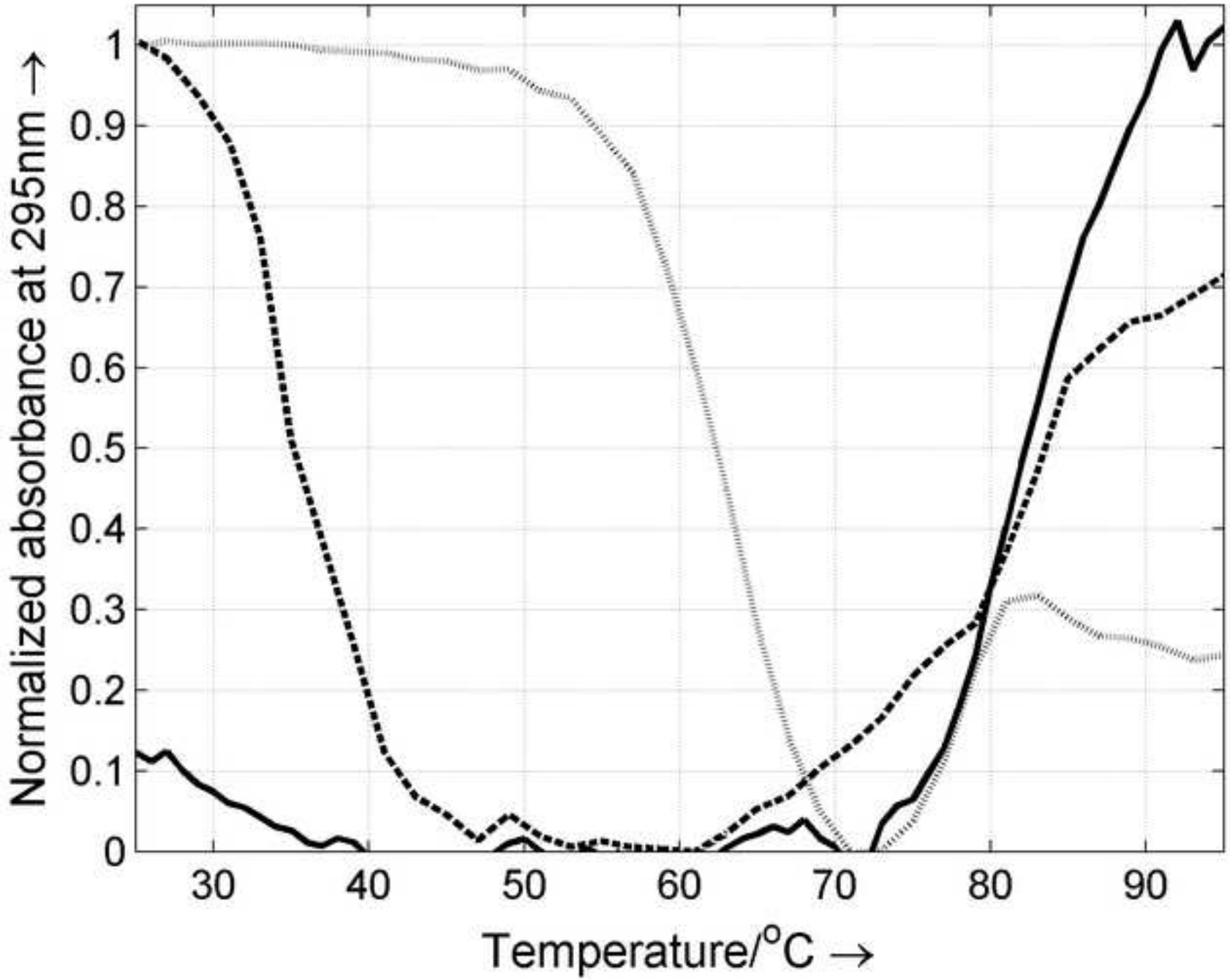
Normalized absorbance at 295nm →
1
0.9
0.8
0.7
0.6
0.5
0.4
0.3
0.2
0.1
0
30
40
50
60
70
80
90
Temperature/°C →

Figure 8

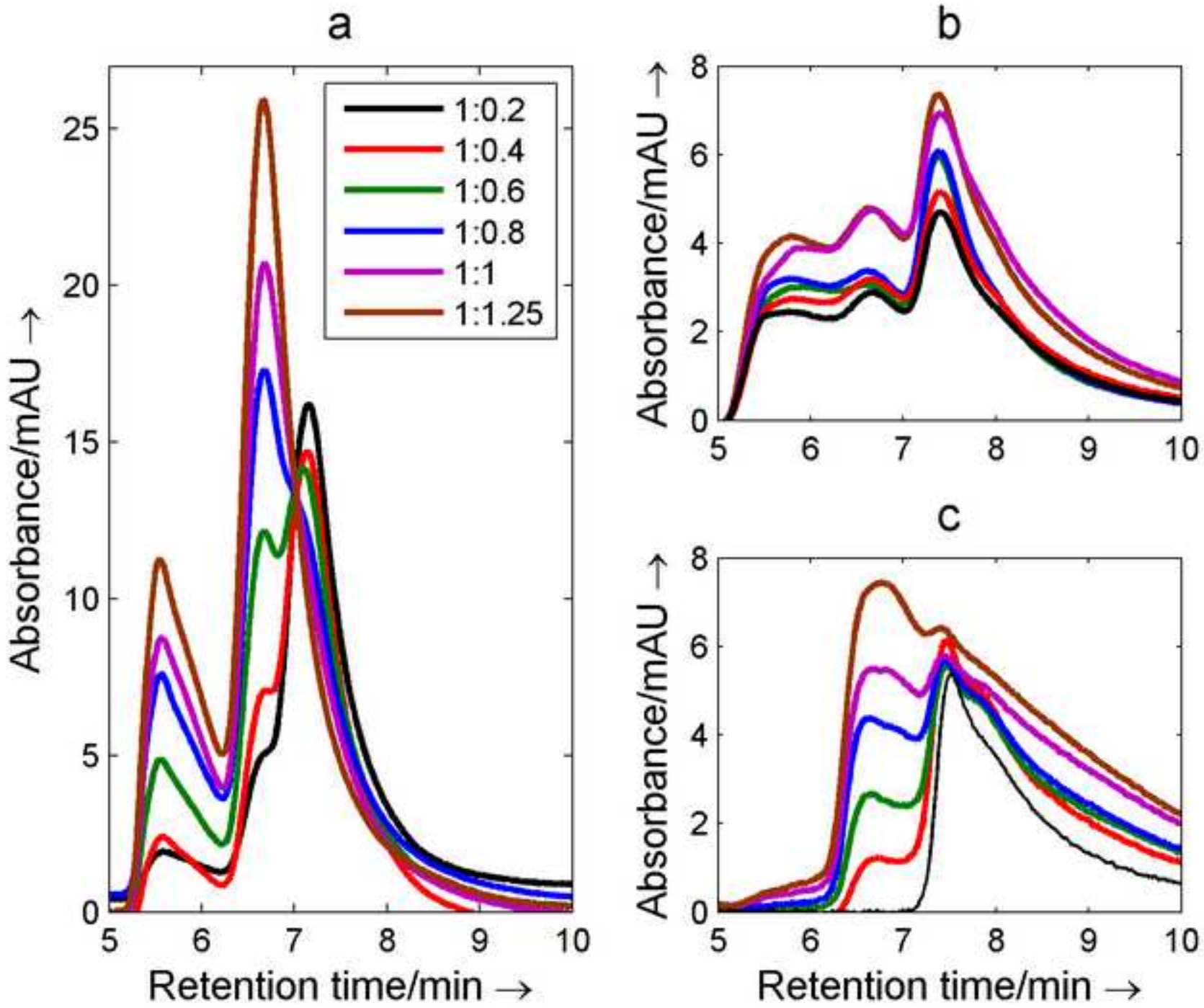
a
b
c
1:0.2
1:0.4
1:0.6
1:0.8
1:1
1:1.25
Absorbance/mAU →
Retention time/min →
0
5
10
15
20
25
2
4
6
8
5
6
7
8
9
10

Figure 9

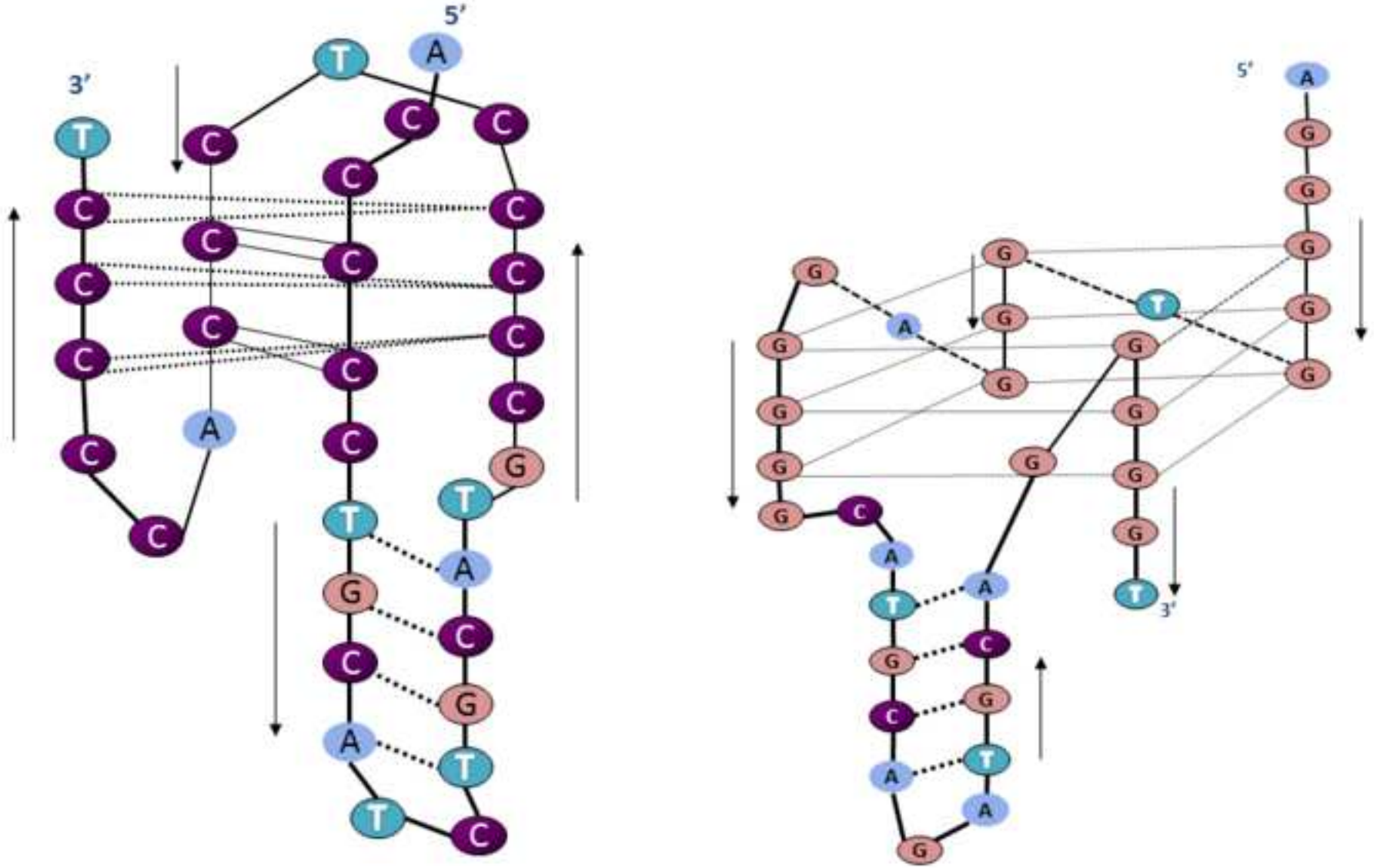

Supplementary Material (for online publication)
Click here to download Supplementary Material (for online publication): Supplementary Material_v4.docx

Supplementary Material

Solution equilibria of cytosine- and guanine-rich sequences near the promoter region of the *n-myc* gene which contain stable hairpins within lateral loops

Sanae Benabou[1], Rubén Ferreira[2], Anna Aviñó[2], Carlos González[3], Sébastien Lyonnais[4], Maria Solà[4], Ramon Eritja[2], Joaquim Jaumot[1], Raimundo Gargallo[1*]

1. Solution Equilibria and Chemometrics Group, Department of Analytical Chemistry, University of Barcelona, Diagonal 645, E-08028 Barcelona, Spain

2. Institute for Advanced Chemistry of Catalonia (IQAC-CSIC), CIBER-BBN Networking Centre on Bioengineering, Biomaterials and Nanomedicine, Jordi Girona 18-26, E-08034 Barcelona, Spain

3. Institute of Physical Chemistry "Rocasolano", CSIC, Serrano 119, E-28006 Madrid, Spain

4. Molecular Biology Institute of Barcelona (IBMB-CSIC), Baldiri Reixac 4-8, 08028 Barcelona, Spain

Contents:

S1. Acid-base titration of nmyc01 sequence.

Whole set of experimental CD and molecular absorption spectra measured along the acid-base titration of nmyc01 sequence:

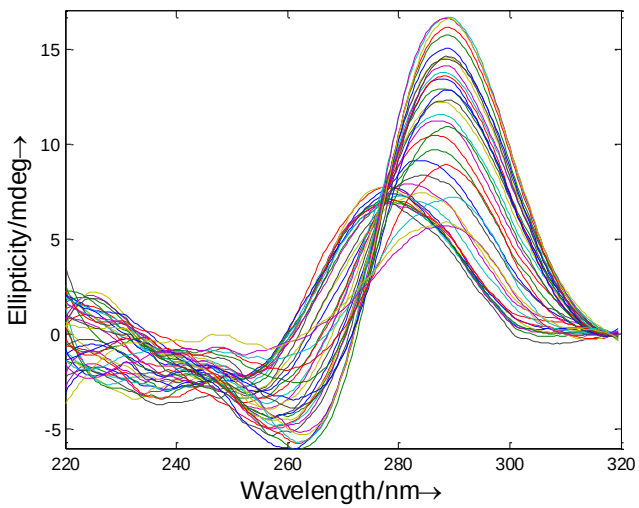

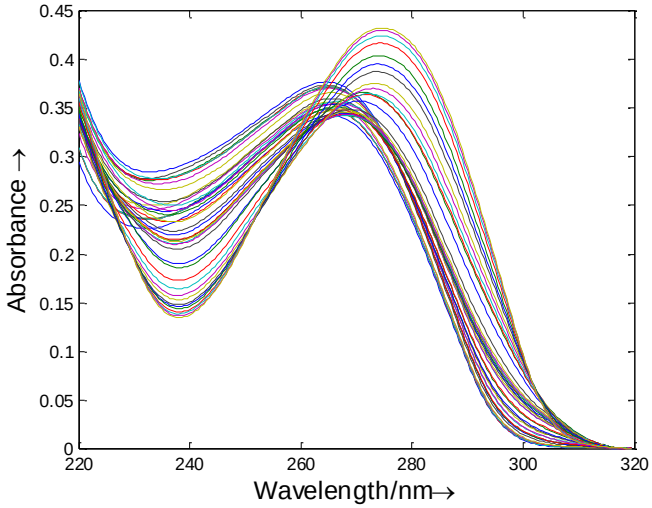

Figure 1c-e showed the results obtained when four species were considered. From the calculated distribution diagram and pure spectra it is possible to calculate the reproduced CD and absorbance data. In this case, the calculated CD signal at 288nm(green line) and the experimental (blue symbols) superimpose, which supports the four-species model.

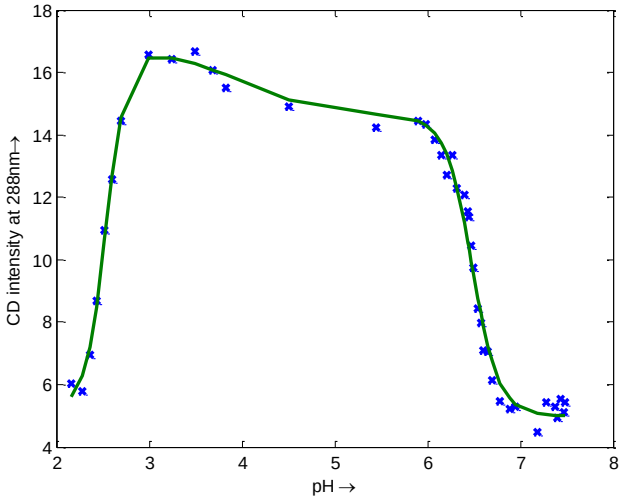

When only three acid-base species were considered, the calculated distribution diagram and fits are shown here. The calculated CD signal at 288nm clearly does not fit the experimental values.

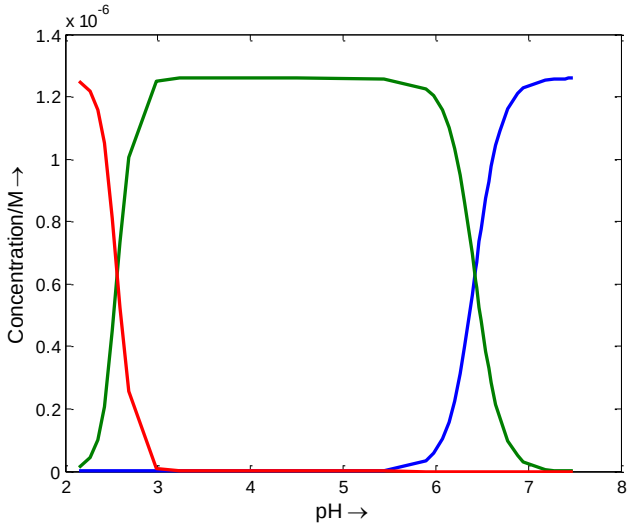

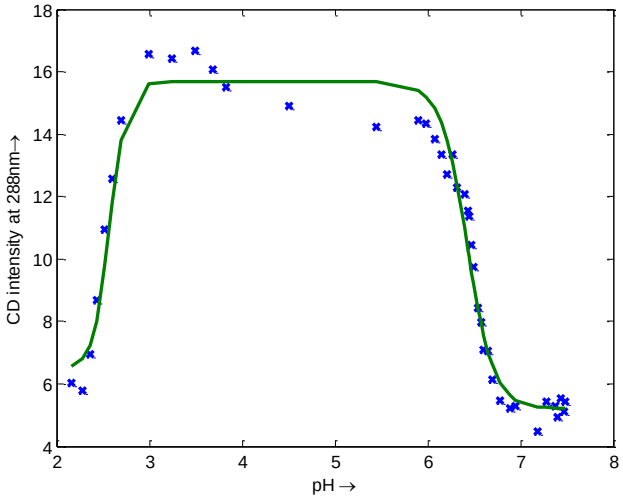

The calculation could not be carried out for a model involving five acid-base species because of rank deficiency problems; the experimental data matrix does not support the addition of more than four components because the rank of the matrix was four.

S2. Melting experiment of nmyc01 at pH 6.1.

Figure S2a shows the spectra recorded during a melting experiment at pH 6.1. The trace at 295 nm indicated a hypochromic transition, characteristic of the unfolding of *i*-motif structures at a pH higher than the pK_a of cytosine, with a transition midpoint around 30°C.

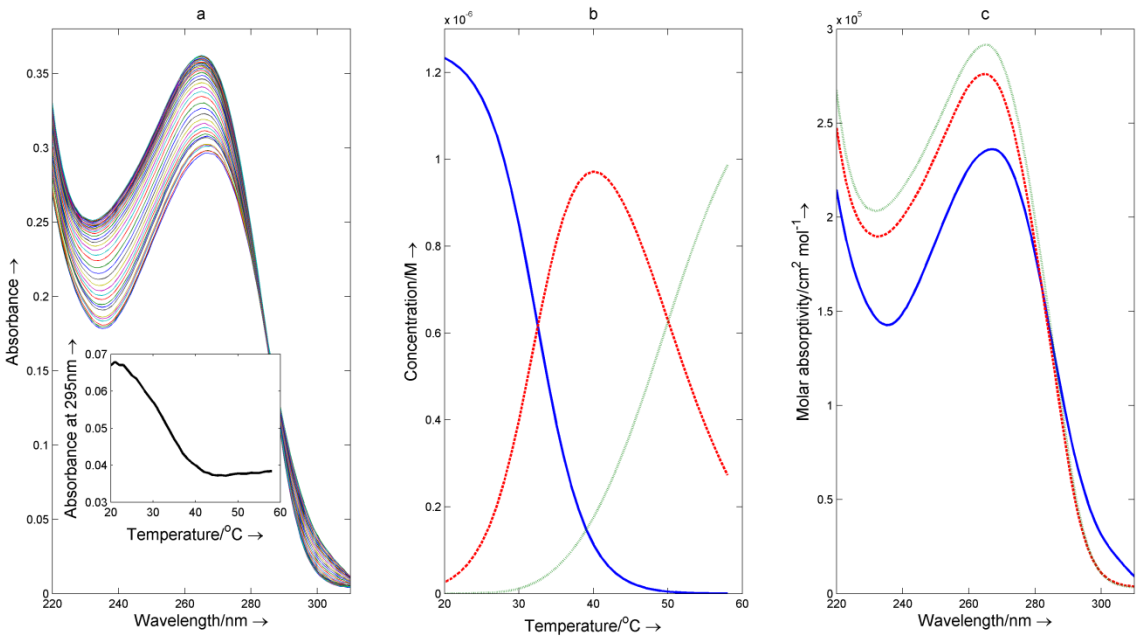

(a) Experimental spectra. Inset: trace at 295nm. (b) Calculated distribution diagram for the three species considered. (c) Calculated pure spectra. Solid blue line: *i*-motif I; dashed red line: partially unfolded strand; dotted green line: completely unfolded strand. C_{nmyc01} = 1.3 μM.

Figure S2b and S2c show the calculated distribution diagram and the pure spectra. Two conformational transitions, i.e., three different species or conformations of nmyc01, were considered. The first transition in Figure S2b, which was accompanied by a large hypochromicity at 295 nm, corresponded to the unfolding of the *i*-motif, which was the major species at pH 6.1 and 20°C, to yield a partially stacked strand. The T_m of this transition was 33±1°C. The calculated changes in enthalpy and entropy were 52 kcal·mol^{-1} and 170 cal·K^{-1}·mol^{-1}, respectively. The second transition, which was mainly denoted by the variation in absorbance at 260 nm, was explained in terms of a loss of stacking upon heating.

The goodness of the proposed model is shown in the experimental *vs.* calculated absorbance values at 295nm next Figure).

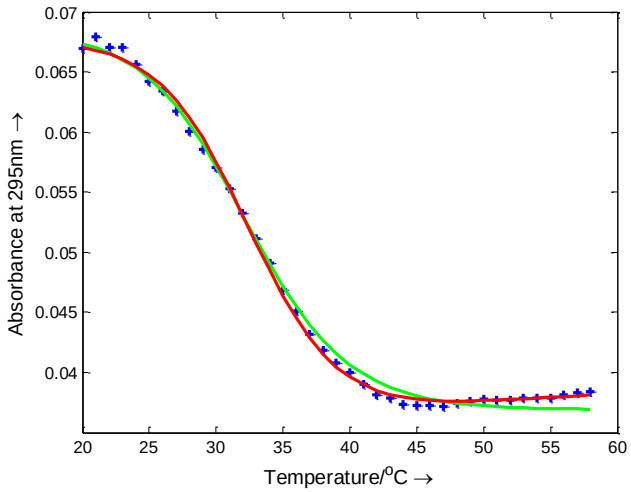

From the calculated distribution diagram and pure spectra it is possible to calculate the reproduced absorbance data. In this case, the experimental trace at 295nm (blue symbols) is superimposed with the calculated traces at 295nm when three (red line) or two (green line) conformations were considered. The model which best fits the experimental data is that considering three conformations.

S3. T_m values determined against pH. Black diamond: myc01; black square: nmyc02.

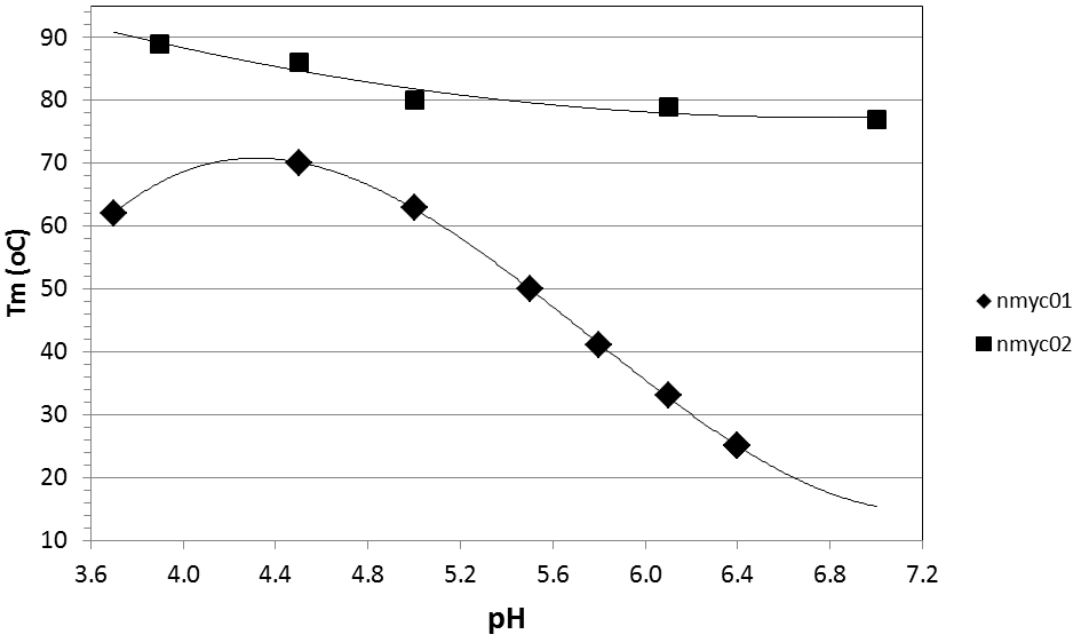

S4. Effect of added KCl on nmyc01 *i*-motif structure.

C_{DNA} was 1.25 µM, 25°C, 20 mM phosphate buffer, pH 6.1.

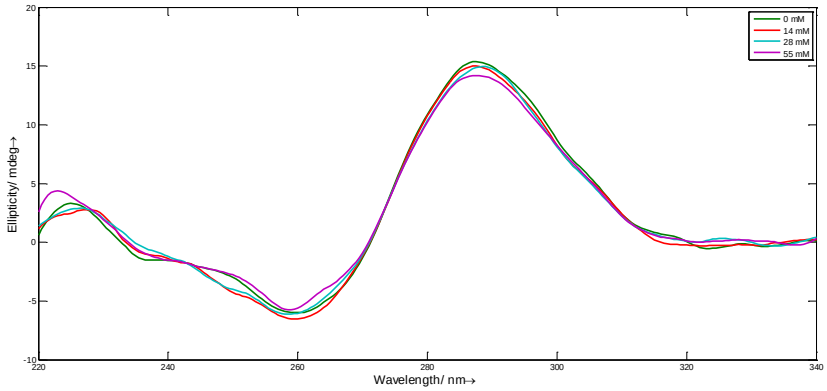

The Tm value at pH 6.1 increased from 33°C (at 150 mM KCl, Figure S2) to 52°C (without added salt, see next figure).

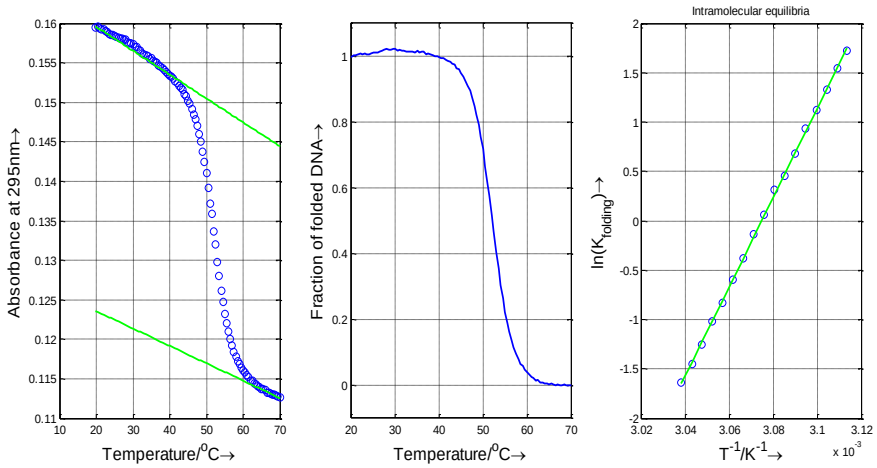

S5. Acid-base titration of nmyc02 sequence.

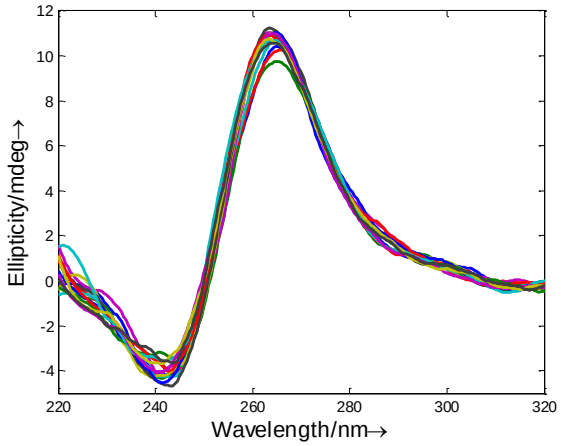

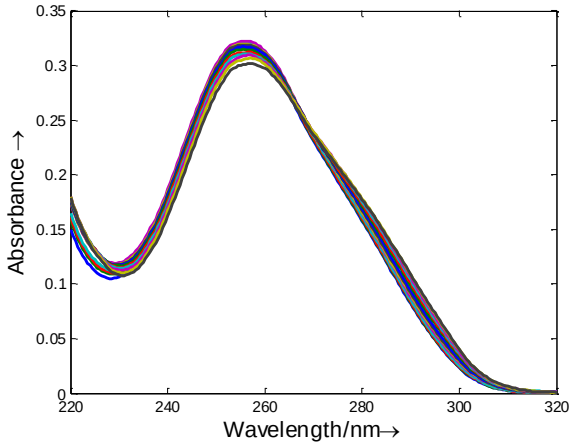

Figure 4c-e showed the results obtained when three species were considered. From the calculated distribution diagram and pure spectra it is possible to calculate the reproduced CD and absorbance data. In this case, the calculated absorbance signal at 295 nm (green line) and the experimental (blue symbols) superimpose, which supports the three-species model.

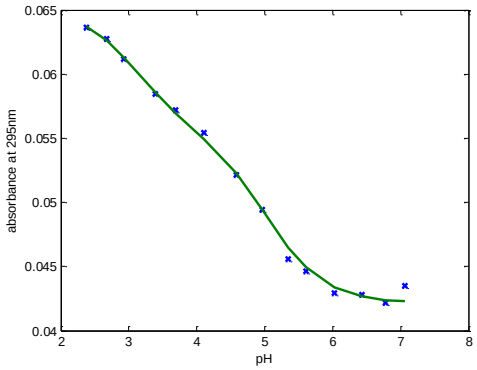

When only two acid-base species were considered, the calculated distribution diagram and fits are shown here. The calculated absorbance signal at 295 nm clearly does not fit the experimental values.

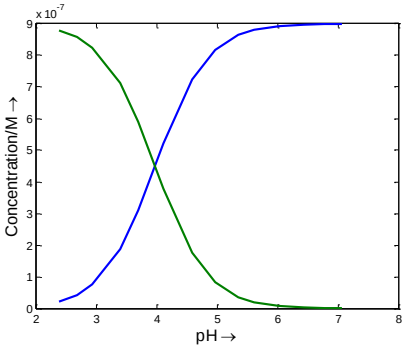

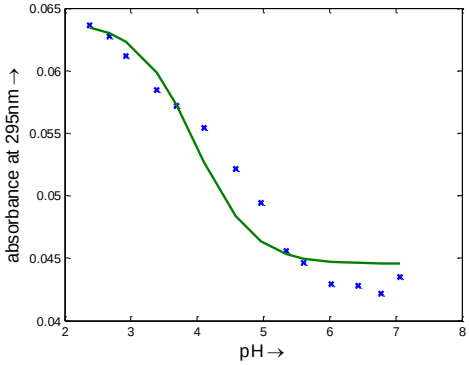

S6. NMR spectra of nmyc02 and nmyc02m sequences.

600-MHz 1H NMR spectra of the exchangeable imino region of nmyc02 (left) and nmyc02m (right) at pH 7.0, and 5.0. All spectra were measured in 100 mM KCl, 25 mM disodium phosphate, 5°C, C_{DNA} = 0.58 mM.

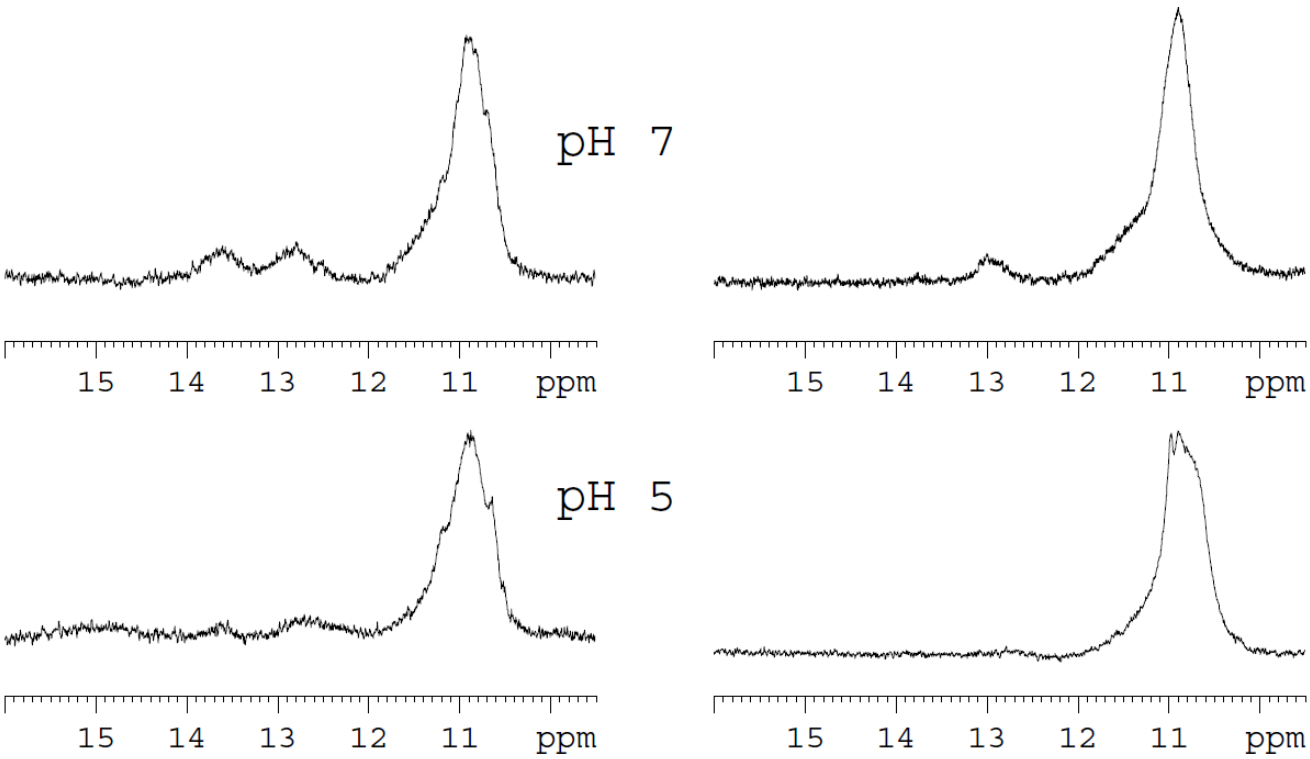

S7. Melting experiment of nmyc02 sequence at pH 6.1.

(a) Experimental spectra. Inset: trace at 295nm. (b) Calculated distribution diagram for the three species considered. Blue: G-quadruplex structure, green: G-quadruplex. Red: completely unfolded nmyc02 strand. (c) Calculated pure spectra. $C_{DNA}=1.7\cdot10^{-6}$ M, pH 6.1.

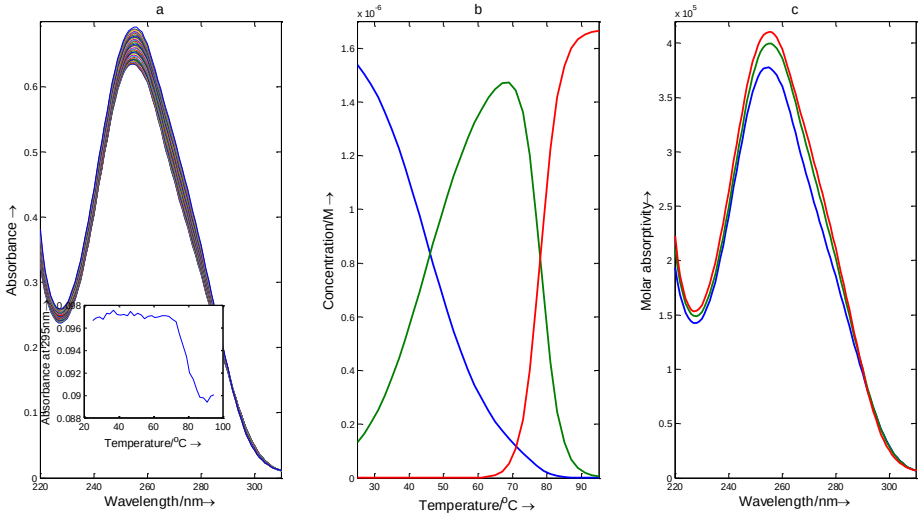

Experimental (symbol) versus calculated (green line) absorbance values at 295nm.

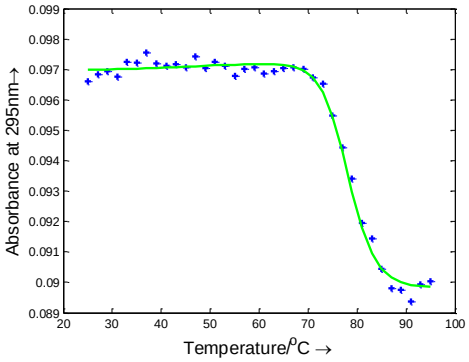

Next figure shows the absorbance traces at 295nm for four nmyc02 concentrations. The first transition is magnified at higher DNA concentrations.

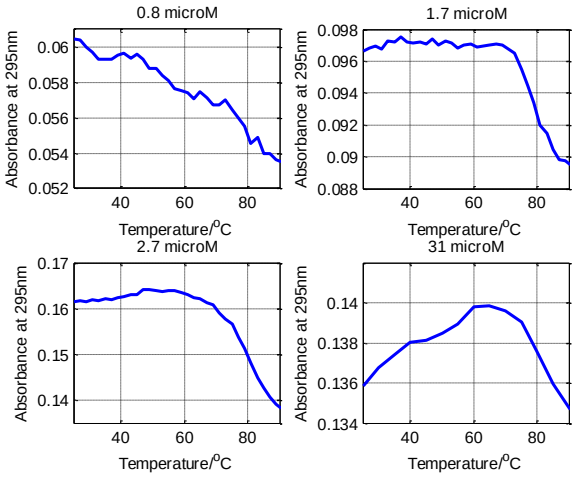

S8. ESI-MS spectrum of the nmyc02 sequence. C_{DNA} was 5 µM, 25 oC, 100 mM ammonium acetate. Other experimental conditions are described in the text.

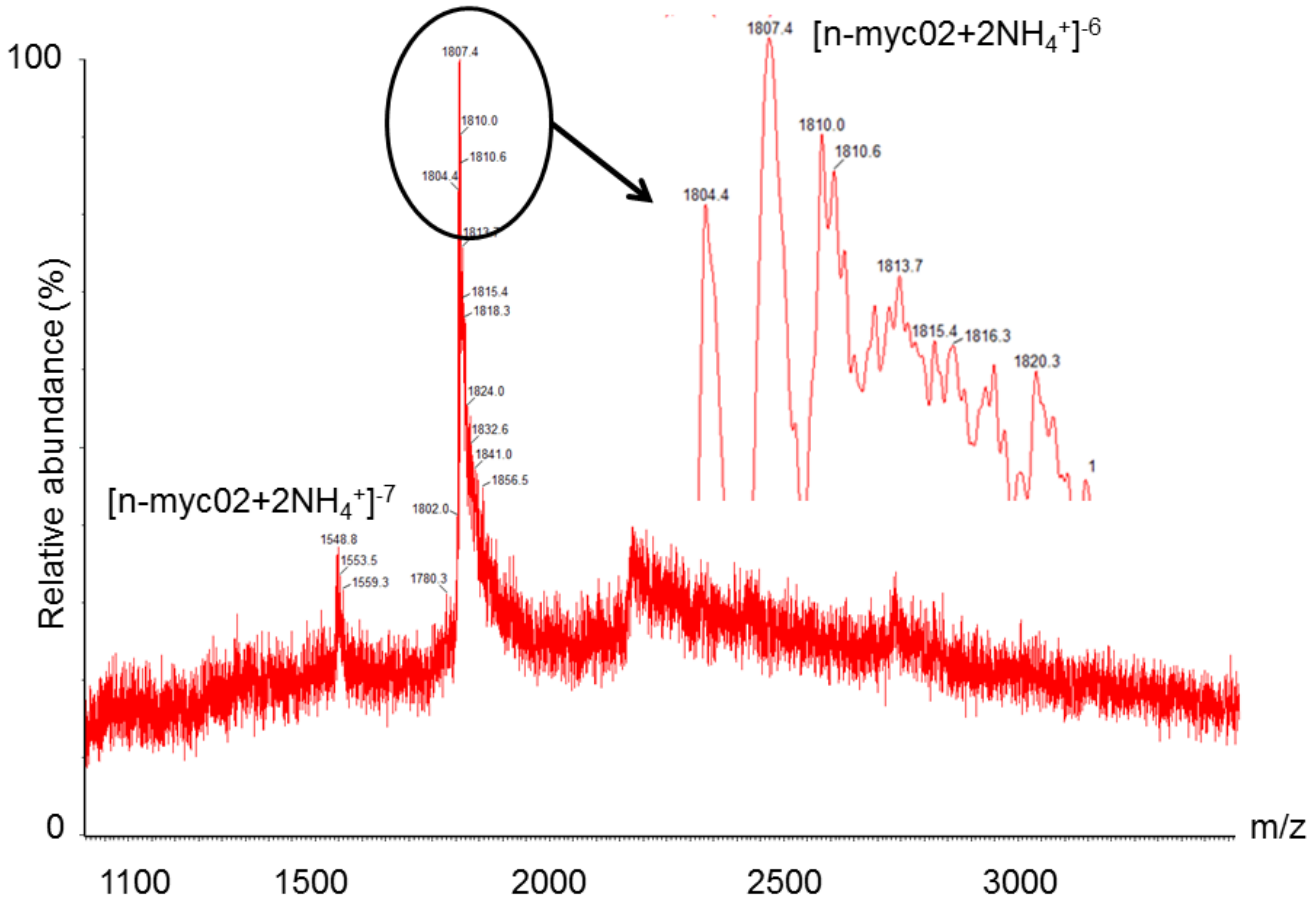

S9. Kinetics of the formation of Watson-Crick duplex at 37°C. C_{nmyc01} = $C_{Fnmy02Q}$ = 2.1 μM.

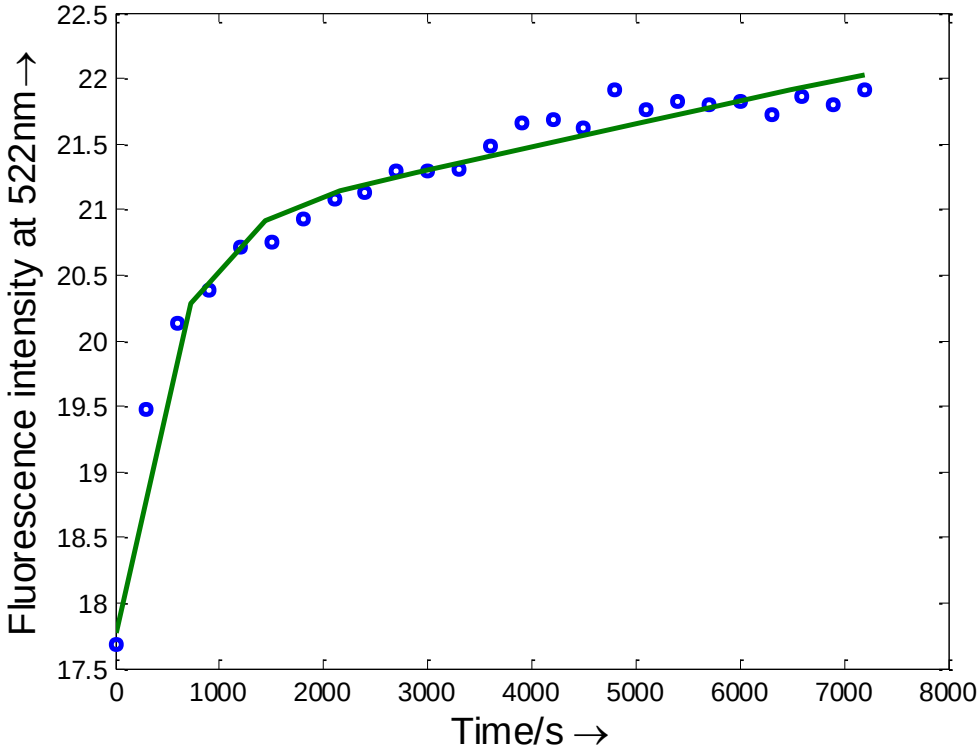

Calculated parameters for the fitting of a double exponential to fluorescence data shown in the previous figure according to the equation:

Fluorescence(t) **= (a*(1-exp(-b*t)))+(c*(1-exp(-d*t)))+e**

Coefficients (with 95% confidence bounds):

a = 2.053 (1.68, 2.427)

b = 0.004623 (0.002935, 0.006311)

c = 2.264 (2.005, 2.522)

d = 0.0004207 (0.0003024, 0.000539)

e = 17.68 (17.52, 17.84)

Goodness of fit:

Sum of Square Errors: 0.1145

R-square: 0.9948

Root Mean Square Error: 0.07567

S10. Acid-base titration of an equimolar mixture of nmyc02 and nmyc01 sequences.

(a) Selected set of CD spectra. (b) Molecular absorption spectra. (c) Fit for CD signal at 288 nm. (d) Fit for absorbance data at 280 nm. Blue: experimental symbols. Green line: fitted data according to the proposed model.